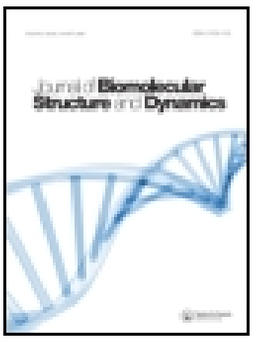

Taylor & Francis
Taylor & Francis Group

Journal of Biomolecular Structure and Dynamics

ISSN: 0739-1102 (Print) 1538-0254 (Online) Journal homepage: https://www.tandfonline.com/loi/tbsd20

Bacterial protein azurin and derived peptides as potential anti-SARS-CoV-2 agents: insights from molecular docking and molecular dynamics simulations

Santanu Sasidharan, Chandrabose Selvaraj, Sanjeev Kumar Singh, Vikash Kumar Dubey, Sachin Kumar, Arsenio M. Fialho & Prakash Saudagar

To cite this article: Santanu Sasidharan, Chandrabose Selvaraj, Sanjeev Kumar Singh, Vikash Kumar Dubey, Sachin Kumar, Arsenio M. Fialho & Prakash Saudagar (2020): Bacterial protein azurin and derived peptides as potential anti-SARS-CoV-2 agents: insights from molecular docking and molecular dynamics simulations, Journal of Biomolecular Structure and Dynamics, DOI: 10.1080/07391102.2020.1787864

To link to this article: https://doi.org/10.1080/07391102.2020.1787864

Published online: 03 Jul 2020.

JOURNAL OF BIOMOLECULAR STRUCTURE AND DYNAMICS
https://doi.org/10.1080/07391102.2020.1787864

Taylor & Francis
Taylor & Francis Group

Bacterial protein azurin and derived peptides as potential anti-SARS-CoV-2 agents: insights from molecular docking and molecular dynamics simulations

Santanu Sasidharan[a], Chandrabose Selvaraj[b], Sanjeev Kumar Singh[b], Vikash Kumar Dubey[c], Sachin Kumar[d], Arsenio M. Fialho[e] and Prakash Saudagar[a]

[a]Department of Biotechnology, National Institute of Technology, Warangal, Telangana, India; [b]Computer Aided Drug Design and Molecular Modeling Lab, Department of Bioinformatics, Alagappa University, Karaikudi, India; [c]School of Biochemical Engineering, Indian Institute of Technology BHU, Varanasi, India; [d]Department of Biosciences and Bioengineering, Indian Institute of Technology Guwahati, Assam, India; [e]Department of Bioengineering, Instituto Superior Técnico, Institute of Bioengineering and Biosciences (iBB), University of Lisbon, Lisbon, Portugal

Communicated by Ramaswamy H. Sarma

ABSTRACT

The current pandemic SARS-CoV-2 has wreaked havoc in the world, and neither drugs nor vaccine is available for the treatment of this disease. Thus, there is an immediate need for novel therapeutics that can combat this deadly infection. In this study, we report the therapeutic assessment of azurin and its peptides: p18 and p28 against the viral structural S-protein and non-structural $3CL^{pro}$ and PL^{pro} proteins. Among the analyzed complexes, azurin docked relatively well with the S2 domain of S-protein compared to the other viral proteins. The derived peptide p18 bound to the active site domain of the PL^{pro} protein; however, in other complexes, lesser interactions were recorded. The second azurin derived peptide p28, fared the best among the docked proteins. p28 interacted with all the three viral proteins and the host ACE-2 receptor by forming several electrostatic and hydrogen bonds with the S-protein, $3CL^{pro}$, and PL^{pro}. MD simulations indicated that p28 exhibited a strong affinity to S-protein and ACE-2 receptor, indicating a possibility of p28 as a protein-protein interaction inhibitor. Our data suggest that the p28 has potential as an anti-SARS-CoV-2 agent and can be further exploited to establish its validity in the treatment of current and future SARS-CoV crisis.

ARTICLE HISTORY
Received 2 June 2020
Accepted 22 June 2020

KEYWORDS
SARS-CoV-2; azurin; p28; coronavirus; molecular dynamic simulation

1. Introduction

Coronavirus (CoV) or Severe Acute Respiratory Syndrome coronavirus (SARS-CoV) has shaken the world since the beginning of the 21st century. The first instance of SARS-CoV spread occurred in 2003 that unleashed a lethality rate of 10% (Cheng et al., 2007; Lee et al., 2003). The second instance, Middle East Respiratory Syndrome Coronavirus (MERS-CoV) outbreak, happened in 2012, which had a lethality rate of 35% (de Groot et al. 2013; Zaki et al., 2012). Both the viruses had zoonotic origin in bats/civets and dromedaries (Lau et al., 2005; Reusken et al. 2013). As of today, no approved drug or vaccine is available for human use against any SARS-CoV. Hence, these viruses pose a severe threat that requires immediate attention. Towards the end of 2019, a new coronavirus was identified and named as "2019-nCoV" by the World Health Organization (WHO) on January 12, 2020. On February 11, 2020, the International Virus Classification Commission (ICTV) classified the 2019-nCoV as Severe Acute Respiratory Syndrome Coronavirus 2 because of its high homology to the SARS-CoV. WHO, in the meantime, christened the disease caused by SARS-CoV-2 as COVID-19 (Chen, Liu, et al., 2020; Zhu et al., 2020). The COVID-19 infected person exhibits several symptoms like fever (88% of total infected), cough (68% of total infected), fatigue (38% of total infected), diarrhea (4% of total infected), vomiting (5% of total infected), and dyspnea (Chen, Zhou, et al., 2020). More severe cases lead to pneumonia, severe acute respiratory syndrome, failure of kidney, and in the worst case, death. There are several drugs and vaccines under various phases of pre-clinical and clinical trials; however, their complete testing and validation will take time. The current critical situation may prevail until any effective drug or vaccine is commercialized (Enayatkhani et al., 2020; Huang et al., 2020). Using established immune-informatics approaches (Kalita et al., 2019; 2020), few epitope-based vaccines have also been developed and found to be successful in eliciting an immune response (Kalita et al., 2020).

CoVs are a large family of enveloped viruses that consist of positive-sense single-stranded RNA and measures a diameter of 80–120 nm. The viruses belong to the Coronaviridae family of the order Nidovirales and are divided into four genera: α, β, γ, and δ (Al-Khafaji et al., 2020). SARS-CoV-2 belongs to the β-genus, and its genome is ∼30 kb in length. The viral genome encodes 16 non-structural and 4 structural proteins among the 29 proteins. The four structural proteins are spike protein (S), envelope protein (E), membrane protein (M), and nucleocapsid protein (N) (Bosch et al., 2003) (Boopathi et al., 2020). Among these proteins, the S-protein,

CONTACT Prakash Saudagar ps@nitw.ac.in Department of Biotechnology, National Institute of Technology, Warangal, Telangana 506004, India

which is conserved in all SARS-CoV-2, is responsible for virion attachment to host angiotensin-converting enzyme-2 receptor (ACE-2 receptor) (Hoffmann et al., 2020). SARS-CoV-2 binds to the ACE-2 receptor with ~10–12-fold higher affinity than SARS-CoV. Though the interactions have been studied in detail, the relation between ACE-2/SARS-CoV-2 binding and the risk of transmission and pathological mechanism of organ damage remains elusive (Kumar et al. 2020). Recent data suggest that SARS-CoV-2 can establish a higher rate of infectivity when it acquires combinatorial mutations at the interfacial residues in the receptor-binding domain (RBD) of S-protein (Padhi et al. 2020)

There are two strategies available to combat this virus. The first one is to prevent the virus by targeting the viral proteins and thereby inhibiting the translation and replication of the virus. The second strategy is to target the human ACE-2 receptor or to build the immune system of the human host. In the first strategy, researches are focused on three approaches (Zumla et al., 2016). The first and foremost approach is the screening of existing broad-spectrum antiviral compounds against the viral proteins (Chan et al., 2013). The second method is to screen for new drug compounds from existing databases, and the latter third approach is to design and develop new therapeutic compounds from scratch (Abdelli et al., 2020; de Wilde et al., 2014; Dyall et al. 2014; Omrani et al., 2014). There have been several attempts to design and develop new drugs against the virus (Elfiky & Azzam, 2020; Gupta et al., 2020; Gyebi et al., 2020; Khan et al., 2020; 2020; Muralidharan et al., 2020; Sarma et al., 2020). Repurposing of several antiviral drugs and peptides are also being conducted (Das et al., 2020; Elmezayen et al., 2020; Islam et al., 2020; Pant et al., 2020; Sinha et al., 2020). The last approach, though potentially useful, is a cumbersome procedure with a timeline of around 10 years (Lobo-Galo et al., 2020). The current study is based on the second approach, wherein we explored the antiviral potential of the bacterial protein azurin and its derivative peptides.

The protein Azurin (14 kDa) secreted by the bacterium *Pseudomonas aeruginosa*, is a widely known copper-containing redox protein. It has a structural similarity with variable domains of immunoglobulins, thereby demonstrating its single antibody-like structure as represented by ribbon drawing of 8 antiparallel strands giving rise to a β-sandwich core, an immunoglobulin fold. The antagonistic activity of full azurin has been established in vitro and in vivo, against cancer (Chakrabarty, 2016), toxoplasmosis (Naguleswaran et al., 2008), malaria (Chaudhari et al., 2006), and most importantly, the protein significantly suppressed the growth of human immunodeficiency virus-1 in peripheral mononuclear blood cells (Chaudhari et al., 2006). Its multivalent therapeutic activity was found to be associated, at least in part, with a 28 amino acid α-helix (p28; L50–D77). Moreover, p18 (an internal p28 fragment; L50–G67) appears to be the minimal motif (protein transduction domain; PTD) responsible for azurin's preferential entry into human cancer cells (Taylor et al., 2009). p28 has completed two phase I clinical trials in cancer patients in the US with no signs of toxicity and with significant tumor regressing effects for some of the patients (Habault & Poyet, 2019).

The current study is directed towards analyzing if azurin and its derived peptides can bind to SARS-CoV-2 proteins computationally. The structure of target proteins $3CL^{pro}$, PLP^{pro}, and spike proteins were retrieved and preprocessed for docking studies. The azurin structure was obtained from the PDB database, and the structure of derived proteins was manually designed. The azurin and the derived peptides p18/p28 were docked against the target proteins of SARS-COV-2, and the results were analyzed for binding affinity. The azurin and its derived peptides were also docked against the ACE-2 receptor to understand if they can inhibit the S-protein/ACE-2 interaction. From the results, we propose that azurin and its derived peptides have high potential as anti-SARS-CoV-2 inhibitors. A representative structure of the azurin and its peptides docked to structural, non-structural, and ACE-2 receptor is shown in Figure 1.

2. Materials and methods

2.1. Target protein structure preparation

For analysis of structure and docking purpose, the structure of viral proteins of SARS-CoV-2 was retrieved from the RCSB protein structure database. The target proteins chosen for this study were two non-structural proteins of the virus: 3 C-like protease ($3CL^{pro}$), papain-like protease (PL^{pro}), and a structural protein: spike protein (S). The choice of proteins was based on previous studies and their role in attachment and replication (Wu et al., 2020). The structure of $3CL^{pro}$ (PDB id: 6M03), PL^{pro} (PDB id: 6W9C), and S-protein (PDB id: 6VYB) were obtained from the RCSB database, and the structures were processed using UCSF Chimera (Pettersen et al., 2004). Processing of the structures involved the removal of water and other heteroatoms from the structures, and clashes in the structure were also refined if any. For docking studies using the ACE-2 receptor, the structure of ACE-2 from *Homo sapiens* (PDB id: 1R42) was obtained and processed, as mentioned before.

2.2. Azurin, p18, and p28 structure preparation

The crystal structure of tetramer protein azurin was retrieved from the RCSB database with PDB id: 1E5Z. The structure was processed, as mentioned previously, using UCSF Chimera. For the preparation of p18 peptide, the region between L50 and G67 of Chain A of 1E5Z was extracted, and the rest of the amino acids were removed. In the case of p28, the peptide fragment between L50 and D77 was taken while the rest of the residues were cleaved off from the structure. The obtained peptide p18 and p28 were processed and analyzed for further docking studies.

2.3. Docking studies using ClusPro and FRODOCK

Once the structures were preprocessed and made ready, azurin and its peptide fragments were docked against the $3CL^{pro}$, PL^{pro}, S-protein, and ACE-2 proteins. For protein-

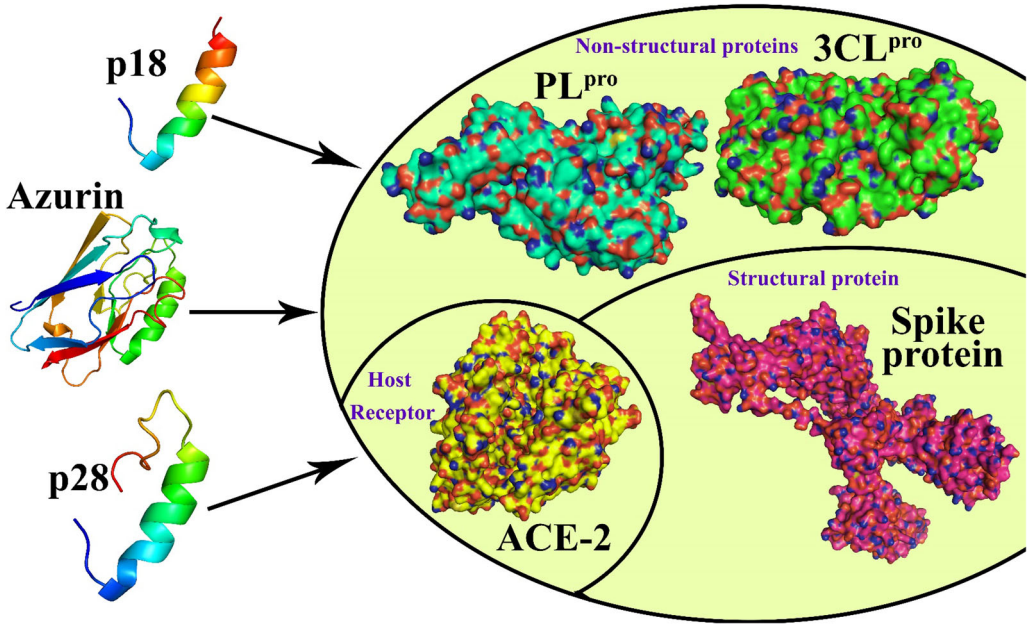

Figure 1. **Representation and workflow of protein molecules involved:** The azurin and its peptides p18 and p28 were docked to structural S-protein, and two non-structural proteins ($3CL^{pro}$ and PL^{pro}) and finally to the human host ACE-2 receptor. The 3 D surface representation of the spike protein, $3CL^{pro}$, PL^{pro}, and ACE-2 can be observed on the right, while the secondary structure representation of azurin and its peptides are provided on the left.

protein docking purposes, two separate servers were employed. ClusPro server 2.0 is a protein-protein docking server that is based on three computational steps, the first involving the rigid-body docking by sampling billions of conformations, the second, root mean square deviation (RMSD) of 1000 lowest energy structures and the final, refining the selected structures by subjecting it to energy minimization (Kozakov et al., 2017; Vajda et al., 2017). In the current study, the docking parameters were maintained as default. The other server for docking was FRODOCK 2.0, which is yet another rigid body based docking algorithm. The server is based on the 3-D grid-based potentials along with the knowledge-based potential and properties of spherical harmonics (SH). This drastically helps in improving the success rates of docking significantly (Garzon et al., 2009; Ramírez-Aportela et al., 2016). The parameters in FRODOCK 2.0 were also set as default for all the docking runs. The first ten models with the lowest energy were selected and visualized using UCSF Chimera (Pettersen et al., 2004) and Discovery Studio R2. All amino acid residue interaction networks were plotted using Cytoscape 3.8 (Shannon et al., 2003).

2.4. Molecular dynamics simulations

MD simulations were performed for the p28 complexed with $3CL^{pro}$, PL^{pro}, S-protein, and ACE-2 proteins for the timescale of 60 nanoseconds (ns) using the GROMACS molecular dynamics package (Selvaraj et al. 2014; Van Der Spoel et al., 2005). The docked complex of $3CL^{pro}$, PL^{pro}, S-protein, and ACE-2 proteins were prepared in a base of the protein-peptide complex. For that, the whole complex was prepared using the OPLS (Optimized Potential for Liquid Simulations) force field, with TIP3P (Transferable Intermolecular Potential with 3 points) water model fixed inside the cubic periodic boundary box, and the distance between the complex structure towards the cubic box was fixed as 1 nm (Nava, 2018; Selvaraj et al. 2014; 2018). These periodic boundary conditions cutoffs for Lennard-Jones and Coulomb interactions set at 1 nm (Qi et al., 2018). Reference temperature for the complex was provided as default 300 K for the thermostat coupling, and Parrinello-Rahman pressure coupling enabled with 1.0 bar reference pressure (Duncan et al., 2016; Sasidharan & Saudagar, 2019). For neutralizing the complex systems, the Na^+/Cl^- ions were added within the system, and the whole complex minimization was performed for removing the initial steric clashes using the steepest descent algorithm via a tolerance of 10 kJ/mol/nm for 1000 steps (Chinnasamy et al., 2020; Shafique & Rashid, 2019). NVT and NPT ensembles are performed with the minimized systems for 1 ns at 300 K and 1 bar pressure (Chinnasamy et al., 2019; Sasidharan & Saudagar, 2020). The minimized complex systems were processed for MD simulation step for the timescale of 60 ns, to determine the stability of the complex systems and the binding energy ($\Delta G_{binding} = E_{gas} + G_{sol} - T\Delta S$) of the complex systems were determined by MM/PBSA calculations for every 20 ns of MD simulations trajectories (Kumari et al., 2014; Shukla et al., 2020).

3. Results

3.1. Analysis of non-structural proteins $3CL^{pro}$ and PL^{pro}

3.1.1. P28 binds to the II and III domain of $3CL^{pro}$ with high affinity

$3CL^{pro}$, also referred to as Nsp5, is the first protein to be cleaved and matured in the virus. The protein is essential for the life-cycle of the virus, wherein it assists the maturation of Nsps (H. Yang et al., 2005). $3CL^{pro}$ has three domains: I (8–101 amino acids), II (102–184 amino acids), and III (201–303 amino acids). The domains II and III are connected

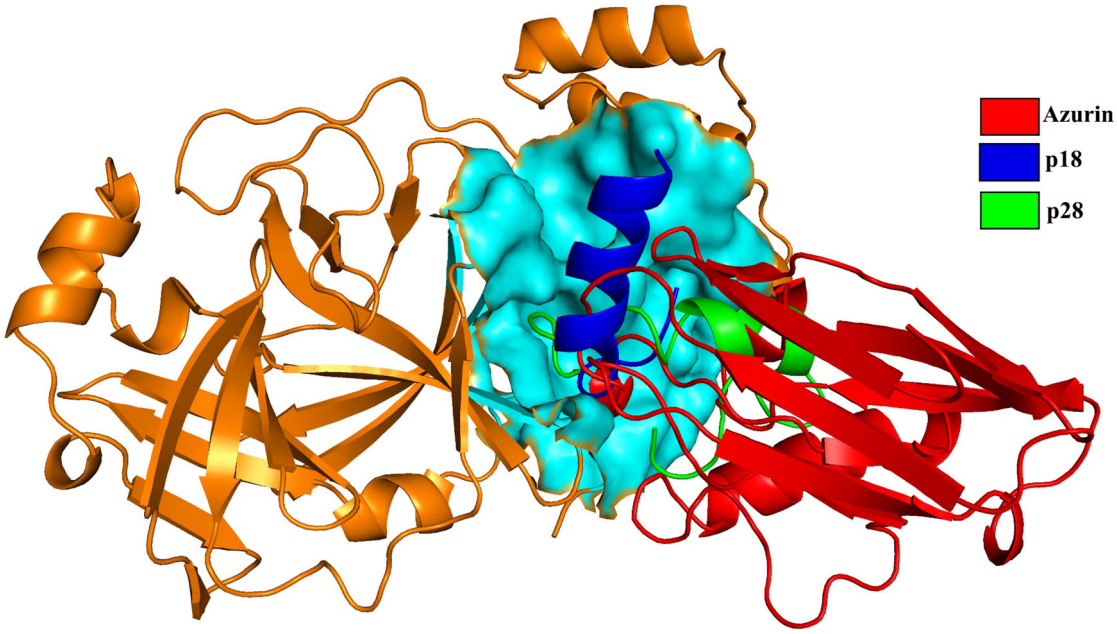

Figure 2. **Docking of azurin and its peptides to 3CL^{pro}:** Azurin and its peptides p18 and p28 docked to the same binding pocket in the 3CL^{pro} domain III. 3CL^{pro} is represented in orange while the surface of the binding site is in cyan.

by a long loop (185–200 amino acids). The active site in the cavity lies between the domains I and II, which includes C145 and H41 (CysHis catalytic dyad) (H. Yang et al., 2003). A graphical representation of azurin, p18, and p28 sharing the domain III binding site is provided in Figure 2. The docking of 3CL^{pro} to azurin using the ClusPro server gave a cluster of 113 members with the lowest energy of −642.4 weighted score. The analysis of the docked protein-protein structure was carried out, and we found the formation of salt bridges, conventional hydrogen bonds, alkyl, pi-sigma, pi sulfur, and pi-alkyl bonds between 3CL^{pro} and azurin. The formation of hydrogen bonds (3CL^{pro}-azurin) were between K101–S89 (2.8 Å), T304–D69 (2.6 Å), D248–Q14 (1.8 Å), D153–N42 (2.2 Å) and T304–D69 (2.4 Å). The pi-sigma and pi-sulfur bonds were between F294–V43 (3.4 Å) and F294–M44 (5.6 Å), respectively. Other interactions between 3CL^{pro}and azurin from ClusPro is given in Figure 3(A). From the FRODOCK server, hydrogen bonds between D153–K41 (3.2 Å) and I249–G116 (3.3 Å) were detected and adding to that salt bridges, alkyl, and pi-alkyl bonds were also present. These interactions detected by FRODOCK are represented in Figure 3(A).

The ClusPro docking analysis between 3CL^{pro} and p18 (3CL^{pro}-p18) gave hydrogen bonds only between R298–A53 (3.2 Å), Q110–Q57 (2.8 Å) and D245–G67 (2.7 Å). The dock had 251 members in the cluster with the lowest energy weighted score value as −699.7. There were alkyl and pi-alkyl interactions between the two proteins, and the interacting residues are represented in Figure 3(B). From the FRODOCK server, only one hydrogen bond between S301–G63 (3.2 Å) and alkyl as well as pi-alkyl bond interactions were observed. The alkyl and pi-alkyl interacting residues are given in Figure 3(B). Varying from azurin and p18, p28 had a high binding affinity to 3CL^{pro} protein wherein a cluster of 106 members was present with the lowest energy being a weighted score of −714.8. The p18 formed several hydrogen bonds like S158–D55 (2.7 Å), Q256–D71 (2.6 Å), R298–S51 (2.8 Å), S301–D71 (2.4 Å), T304–D76 (2.4 Å), D295–L50 (1.9 Å), D295–S51 (2.1 Å), F294–S51 (1.8 Å), N151–A53 (2.9 Å) and I152–T52 (3.3 Å). Along with the hydrogen bond formation between residues, there were other interactions like electrostatic, pi-sigma, alkyl, and pi-alkyl, which are tabulated in Figure 3(C). According to the FRODOCK server, L50 and K102 of p28 interacted with D248 and D69 of 3CL^{pro} by hydrogen bond and, electrostatic as well as alkyl interactions were also observed (Figure 3(C)).

3.1.2. P28 interaction with PL^{pro} is well stabilized by electrostatic, alkyl, and hydrogen bonds

PL^{pro} is an essential enzyme in the virus that cleaves replicase N-terminus. This, in turn, releases Nsp1, Nsp2, and Nsp3, which are responsible for virus replication and also inhibit the host's innate immunity (Chen et al., 2014; Harcourt et al., 2004; Li et al., 2016). Figure 4 shows the binding of azurin to the UBL (ubiquitin-like domain), p18 to the active site cavity, and p28 to the finger domain. ClusPro docking of PL^{pro} with azurin resulted in a cluster of 103 members with the lowest energy of −526.4 weighted score. Analyzing the structure, hydrogen bond interactions (PL^{pro}-Azurin) were observed betweenY137–Q12 (2.7 Å), Y137–Q14 (2.5 Å), and I14–Y72 (1.8 Å). There were several alkyl hydrophobic interactions between L16, P130, A141, R138 of PL^{pro}and L68, L39, L120, A119 of PL^{pro}, respectively. Pi-alkyl interactions were also formed, as shown in Figure 5(A). From FRODOCK server, hydrogen bond interactions between Y171–Q107 (2.3 Å), M208–T61 (2.3 Å), C224–Y72 (3.1 Å), Y171–Q107 (2.8 Å), R225–N42 (3.5 Å), Y171–T52 (3.2 Å) and Q195–G116 (2.7 Å) were visualized. Aside from hydrogen bond interactions, electrostatic interactions, alkyl, and pi alkyl interactions were also present between the proteins (Figure 5(A)).

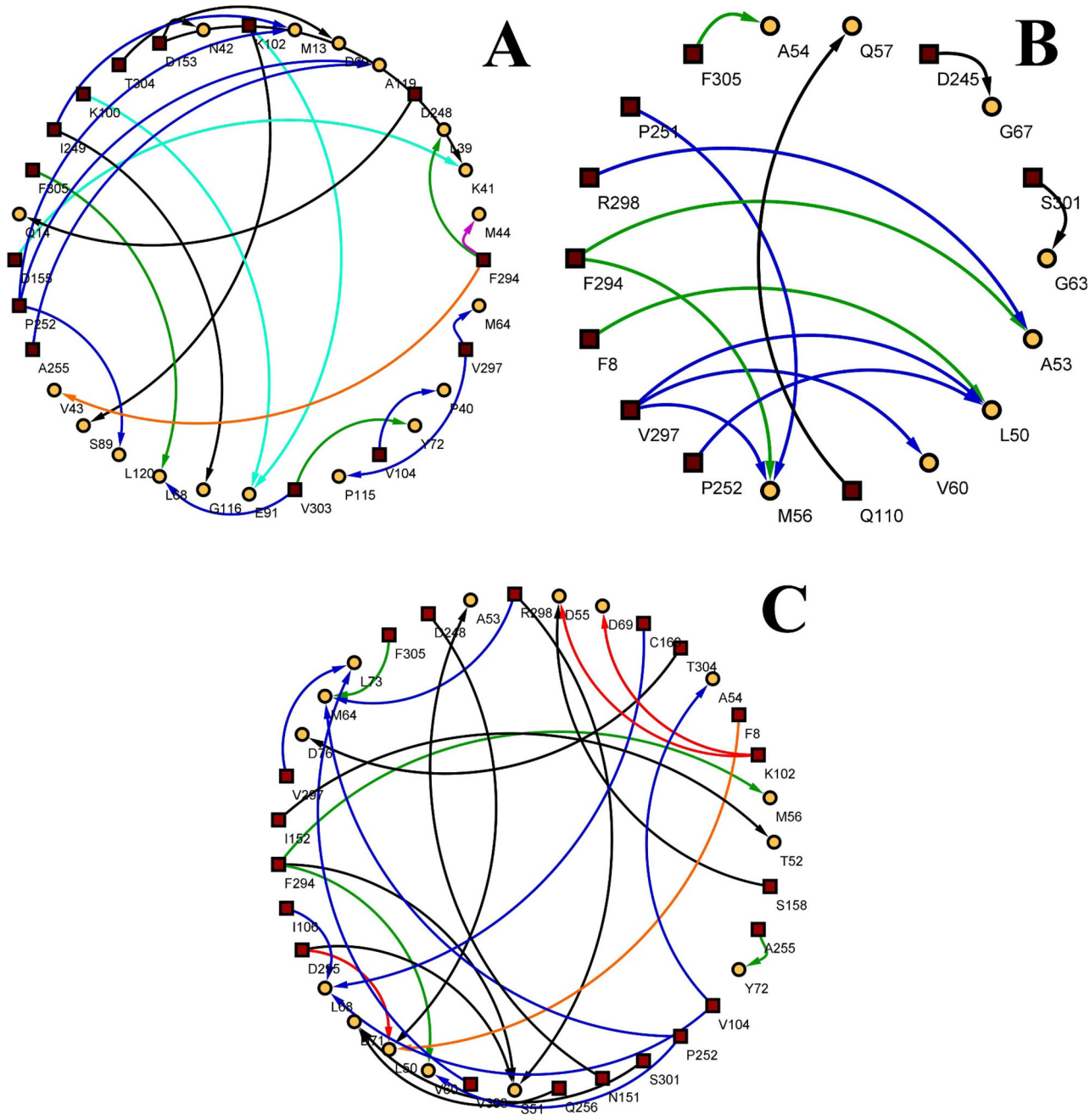

Figure 3. Residue interaction network between 3CL^{pro} and azurin/p18/p28: Among the interactions analyzed, p28 bound more to the 3CL^{pro} by several diverse bond formations. **(A)** Residue interactions between 3CL^{pro}and azurin. **(B)** Residue interactions between 3CL^{pro} and p18. **(C)** Residue interactions between 3CL^{pro} and p28. 3CL^{pro} is represented in brown square boxes, and docked molecules are shown in yellow circles. Interactions are colored based on their type: Alkyl (blue); Electrostatic (red); Hydrogen bond (black); pi-alkyl (green); pi-sigma (orange); pi-sulfur(magenta); salt bridges (cyan).

When p18 was docked to PL^{pro} using ClusPro server, A288, D286, and G287 of PL^{pro} formed hydrogen bonds with S51, S51, and L50, at a distance of 3.0 Å, 1.6 Å and 3.2 Å, respectively. The cluster size was of 291 members with −607.3 as the lowest energy weighted score. V59 of p18 formed extensive pi-sigma interaction with W106 and H272. There were electrostatic, alkyl as well as pi alkyl bonds betweenK105, D286, C111, A114, C270, L289 and H272 of PL^{pro} and the first 10 amino acid residues of p18 (Figure 5(B)). The FRODOCK server results suggested a different binding site where the N13, K53, R138, and D12 bonded to S51 (3.3 Å), Q57 (3.2 Å), L50 (2.6 Å) and L50(2.3 Å), respectively. The interaction of p18 was restricted entirely to the N-terminus and also interacted by pi-sulfur, alkyl, and pi-alkyl interactions, as presented in Figure 5(B). With a cluster size of 169 members, p28 docked PL^{pro} with the lowest energy of −700.3 weighted score. Interestingly, as observed in 3CL^{pro}, p28 interacted effectively with PL^{pro,} and the interactions were stabilized by a balance of hydrogen bonds and alkyl bonds. Hydrogen bond interactions included Y171–D76 (3.1 Å), K232–D71 (2.6 Å), N267–A53 (2.0 Å), Q195–Y72 (2.6 Å) and N267–T52 (3.1 Å). In addition to it, a salt bridge between K232–D71(3.4 Å) and pi-sigma interaction between I222–Y72 (3.4 Å) was also observed to be formed, as shown in Figure

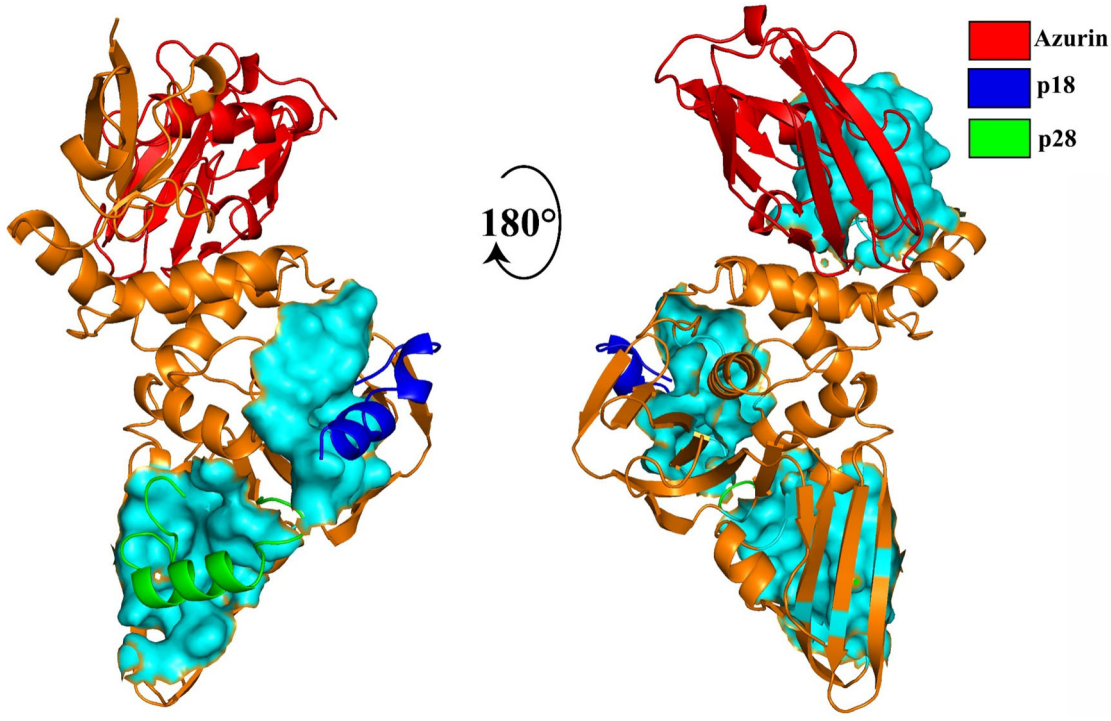

Figure 4. Docking of azurin and its peptides to PL^{pro}: Azurin and its peptides p18 and p28 had different binding pockets in PL^{pro,} as observed in the figure. PL^{pro} is represented in orange while the surface of the binding site is in cyan. Azurin (red) bound to the UBL domain of PL^{pro} while p18 (blue) targeted the active site cavity. p28, on the other hand, can be seen binding to the finger domain of PL^{pro,} which houses the catalytic zinc ion.

5(C). The FRODOCK server results supported the ClusPro findings, and pi-sigma interaction between H73–M64; also, pi-pi stacked interactions between F69–Y72 were detected. Furthermore, alkyl and pi-alkyl bonds were also reported in the FRODOCK results (Figure 5(C)).

3.2. Azurin and p28 preferentially binds to the large spike protein

Spike protein is a vital structural protein that helps the virus gain entry into the host by receptor binding (Hasan et al., 2020). In this virus, the receptor of interest is the ACE-2 receptor present in humans. For viral invasion and tissue of binding determination, S protein gets cleaved into S1 and S2 by host cell proteases. S1 is responsible for binding to host cell surface receptors while S2 mediates virus-cell and cell-cell fusion of membranes (Xia et al., 2014). The receptor-binding domain of the spike protein lies between the 331–524 region of the S-protein (Tai et al., 2020). Azurin was docked against S-protein in ClusPro, and multiple intermolecular hydrogen bonds were confirmed: R1107–L120 (3.1 Å), N1108–Q14 (2.7 Å), S1123–Q57 (2.9 Å), Y1047–N10 (2.6 Å), I909–Q14 (2.3 Å), Y707–N42 (2.2 Å), Y707–V43 (2.7 Å), S1123–Q57 (1.8 Å), R1091–K122 (1.7 Å), R1107–Q12 (2.6 Å), and P1079–G116 (3.3 Å). The lowest energy recoded was −751.5 weighted score, and the cluster size was 126 members. The azurin bound to the S2 domain of the S-protein is presented in Figure 6. The S-protein also interacted with azurin by pi-sigma, alkyl, and pi-alkyl bonds Figure 7(A). FRODOCK docking analysis corroborated the ClusPro server results and further characterized the presence of Y707–P115 (3.15 Å), R1039–D6 (2.9 Å), R1107–L120 (2.9 Å), R1107–F15 (3.7 Å), V1129–Q57 (3.2 Å) and G1093–K122 (3.1 Å) hydrogen bonds. Furthermore, alkyl and pi-alkyl bonds between S-protein and azurin were also established, as plotted in Figure 7(A).

With a cluster size of 200 members and the lowest energy of −733.5 weighted score, p18 docked to S-protein set up hydrogen bonds inter-molecularly between R319–S66 (2.3 Å), T549–G67 (2.6 Å), R567–T52 (2.7 Å), T573–L50 (2.8 Å) and L517–A53 (1.8 Å). Additionally, from the ClusPro server analysis, R567–D55 salt bridge, R567–D55 electrostatic, F565–L50 pi-alkyl bonds, and alkyl bonds were also present in Figure 7(B). FRODOCK server results expounded the manifestation of hydrogen bonds between S-proteins Y707, N1108, G910, Y1047, and p18's A54, M64, G67, and A65, respectively. Only alkyl bond formation was detected apart from the hydrogen bonds in the results of FRODOCK (Figure 7(B)). The peptide fragment p28 docked to S-protein gave a cluster of 184 members, and the lowest energy in the cluster was of −809.7 weighted score. Similar to the binding in 3CL^{pro} and PL^{pro}, p28 bound with high affinity to S-protein too. But fascinatingly, unlike azurin and p18, p28 bound to the N-terminal region of the S-protein with intermolecular hydrogen bond between R214, A67, D138, D138, Y28, P82, R214 of S-protein and L68 (2.17 Å), L50 (1.9 Å), A53 (2.4 Å), A54 (1.8 Å), Y72 (1.9 Å), A53 (3.7 Å), D71 (2.6 Å) of p28, respectively. p28 also formed electrostatic, pi-sigma, pi-sulfur, alkyl, and pi-alkyl bonds with S-protein (Figure 7(C)). G412–D69 (3.25 Å), Q134–Y72 (2.6 Å), and F135–Y72 (3.5 Å) hydrogen bonds were determined in the FRODOCK server analysis. The R102–D71 salt bridge, along with alkyl and pi-alkyl interactions, were also detected towards the N-terminal of S-protein. The binding pattern was similar to the ClusPro

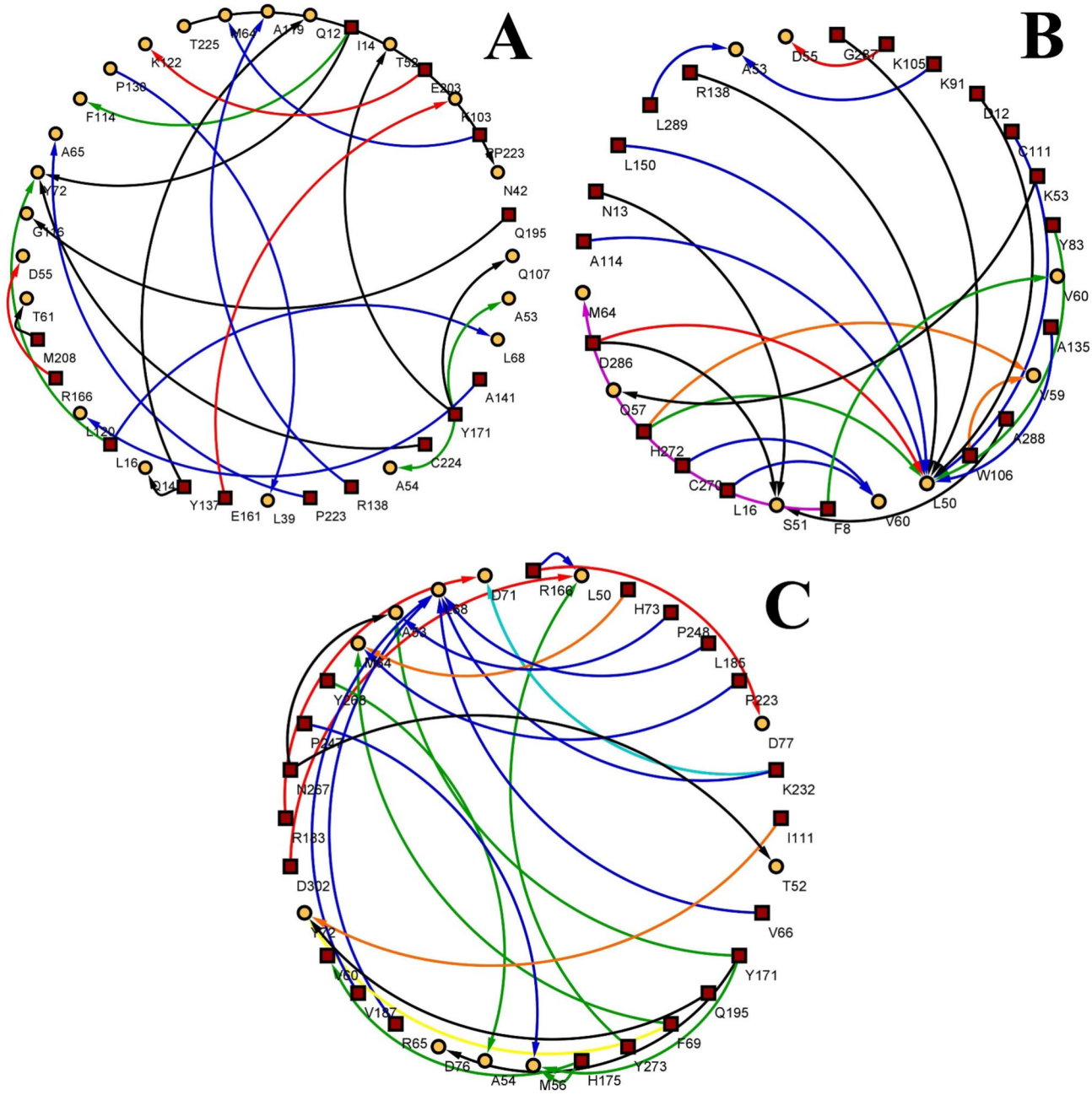

Figure 5. **Residue interaction network between PL^{pro} and azurin/p18/p28:** The residue network explains the good binding propensity of azurin as well as p18 and p28 to PL^{pro}. **(A)** Residue interactions between PL^{pro} and azurin. **(B)** Residue interactions between PL^{pro} and p18. **(C)** Residue interactions between PL^{pro} and p28. PL^{pro} is represented in brown square boxes, and docked molecules are shown in yellow circles. Interactions are colored based on their type: Alkyl (blue); Electrostatic (red); Hydrogen bond (black); pi-alkyl (green); pi-sigma (orange); pi-sulfur(magenta); pi-pi (yellow); salt bridges (cyan).

results and, therefore, substantiated the binding affinity of p28 to S-protein (Figure 7(C)). The p18 and p28 bound to the S1 N-terminal and S1 C-terminal, respectively, can be observed in Figure 6.

3.3. P28 is capable of binding to the ACE-2 N-terminal-peptidase domain by alkyl interactions

The current research shows that ACE-2 is the receptor that helps the entry of SARS-CoV-2 into the host, and this was consistent with the SARS-CoV receptor identified. The receptor-binding domain of SARS-CoV and SARS-CoV-2 are similar with respect to the receptor-binding domain. With this reason as the basis, ACE-2 can also be a target in the host, thereby preventing the entry of the virus into host cells. ACE-2 has an N-terminal peptidase domain that binds to the RBD of the spike, a C-terminal collectrin-like domain followed by a single transmembrane helix and a 40 residue intracellular segment at the end. The ClusPro analysis of ACE-2 docked with azurin gave a cluster of 130 members, and the lowest energy recorded was −605.3 weighted score. The intermolecular hydrogen bonds were between R559 and Q552 of ACE-2 and M64 (2.8 Å), S66(3.1 Å), N42 (2.6 Å), Y72 (3.7 Å) of azurin respectively. The azurin docked to the ACE-2 receptor complex is represented in Figure 8. The docking results,

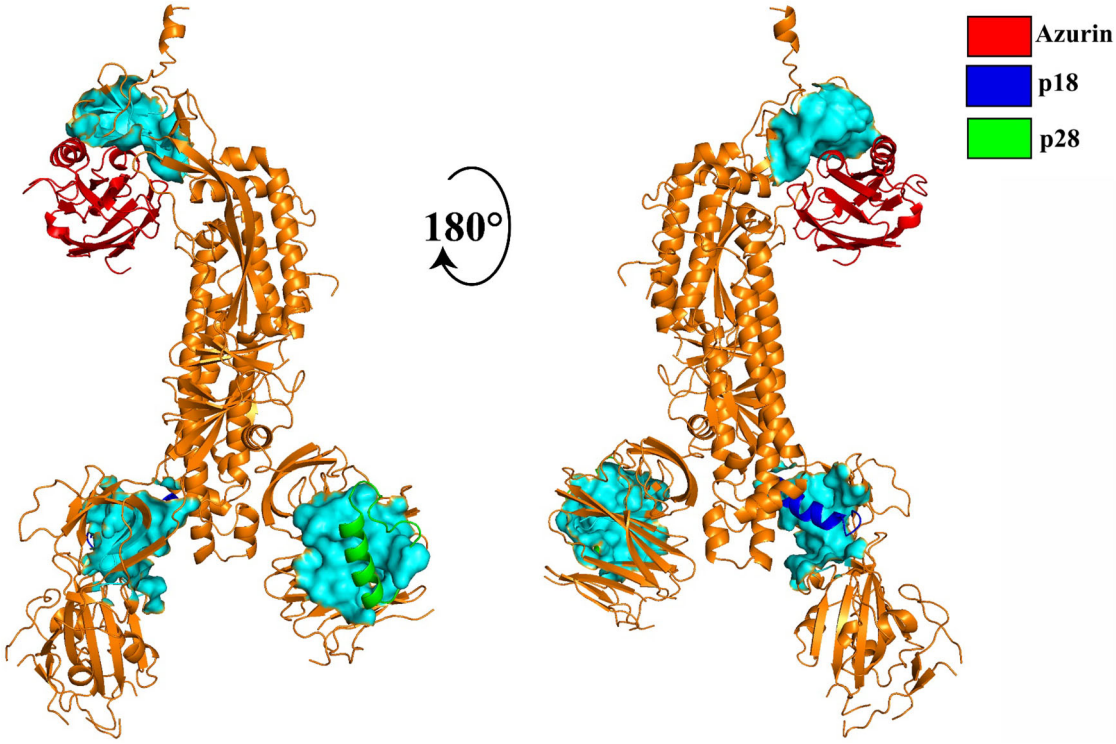

Figure 6. Docking of azurin and its peptides to S-protein: S-protein is represented in orange while the surface of the binding site is in cyan. Azurin (red) bound to the S2 domain of the spike protein, which is responsible for the fusion of the virus to the target. p18 and p28 targeted the S1 (N-terminal) and S1 (C-terminal) of the spike protein, and this S1 domain contains the RBD for ACE-2 receptor binding.

other than the hydrogen bonds, displayed electrostatic, pi-pi stacking, alkyl, and pi-alkyl interactions (Figure 9(A)). FRODOCK server results defined the hydrogen bonds between K353, A387, L320, Q552, G319 and P321 of ACE-2 and N38 (3.2 Å), Q12 (3.3 Å), Y72 (2.9 Å), G116 (3.3 Å), M64 (3.7 Å) and Y72 (2.8 Å) of azurin protein, respectively. Only alkyl and pi-alkyl bonds were determined, as shown in Figure 9(A).p18 docking to ACE-2 using ClusPro gave a cluster member size of 188 and lowest energy weighted score as −708.1. There was only one hydrogen bond between R273 and R52 at a distance of 3.7 Å. Most of the interactions between the proteins were mostly pi-alkyl, and the interactions are recorded in Figure 9(B). FRODOCK analysis also gave only one intermolecular hydrogen bond between A348 and S66 (3.3 Å of p18) and one pi-sulfur interaction between M56 and F504. Apart from these, most of the interactions seen were pi-alkyl and alkyl (Figure 9(B)). The third peptide p28, when docked to ACE-2, exhibited a cluster of 241 members and −887.6 lowest energy weighted score. The stabilization of the protein-protein complex was by hydrogen bonds, pi-sigma, and pi-alkyl interactions mostly. In this complex, hydrogen bonds were between N51–M64 (3.2 Å), D350–Q57 (2.8 Å), N394–S51 (1.8 Å), N508–D76 (2.5 Å) and P346–Y72 (3.0 Å). Salt bridge formation was observed between R273 and D71, while pi-sulfur interactions were between W349 of ACE-2 and M64 of p28. From the docking of p28, the peptide bound to residues of the N-terminal by alkyl interactions, and this domain was responsible for the peptidase activity (Figure 8). FRODOCK server analysis gave strong support to the ClusPro results of p28–ACE-2, wherein hydrogen bonds between W69–A53 (3.0 Å), N508–K74 (3.3 Å), V343–D71 (3.1 Å) and W349–L50 (3.7 Å) (Figure 9(C)). As observed in ClusPro, p28 bound to the N-terminal by alkyl interactions peptidase domain, which facilitated the binding of the RBD region of the spike protein.

4. Molecular dynamics simulations

Based on the docking and interaction patterns, we hypothesize that the p28 could be a strong and potent inhibitor against the SARS-CoV-2 proteins. To justify our findings, we simulated the p28 peptide, complexed with the $3CL^{pro}$, PL^{pro}, S-protein, and ACE-2 proteins, for 60 ns of timescale. The purpose of the simulations was to understand the binding stability of the protein-peptide complex and to understand the energy values in the dynamics. With reference to the original docked pose of the complex, the deviations of each snapshot from the trajectories were marked throughout the MD simulations and plotted in Figure 10. The p28 peptide – ACE-2 complex represented in black color, showed limited deviations till 18^{th} ns of simulations and attained the equilibrium by exhibiting stable conformations. The level of the RMSD snapshots for p28 peptide – ACE-2 complex was present in between the ∼0.25 nm to ∼0.3 nm. Compared to the deviations of ACE-2 peptide complex, $3CL^{pro}$ and PL^{pro} had higher deviations, which indicated that the p28 bound inside the $3CL^{pro}$ and PL^{pro} was active in conformational changes. But the overall simulation confirmed the stable conformations by positioning the RMSD values between ∼0.25 nm to ∼0.33 nm for $3CL^{pro}$, and ∼0.25 nm to 0.37 nm for PL^{pro}. Strong binding between the p28 complexes with spike protein was noticed in the MD simulations, that allocated the RMSD positions

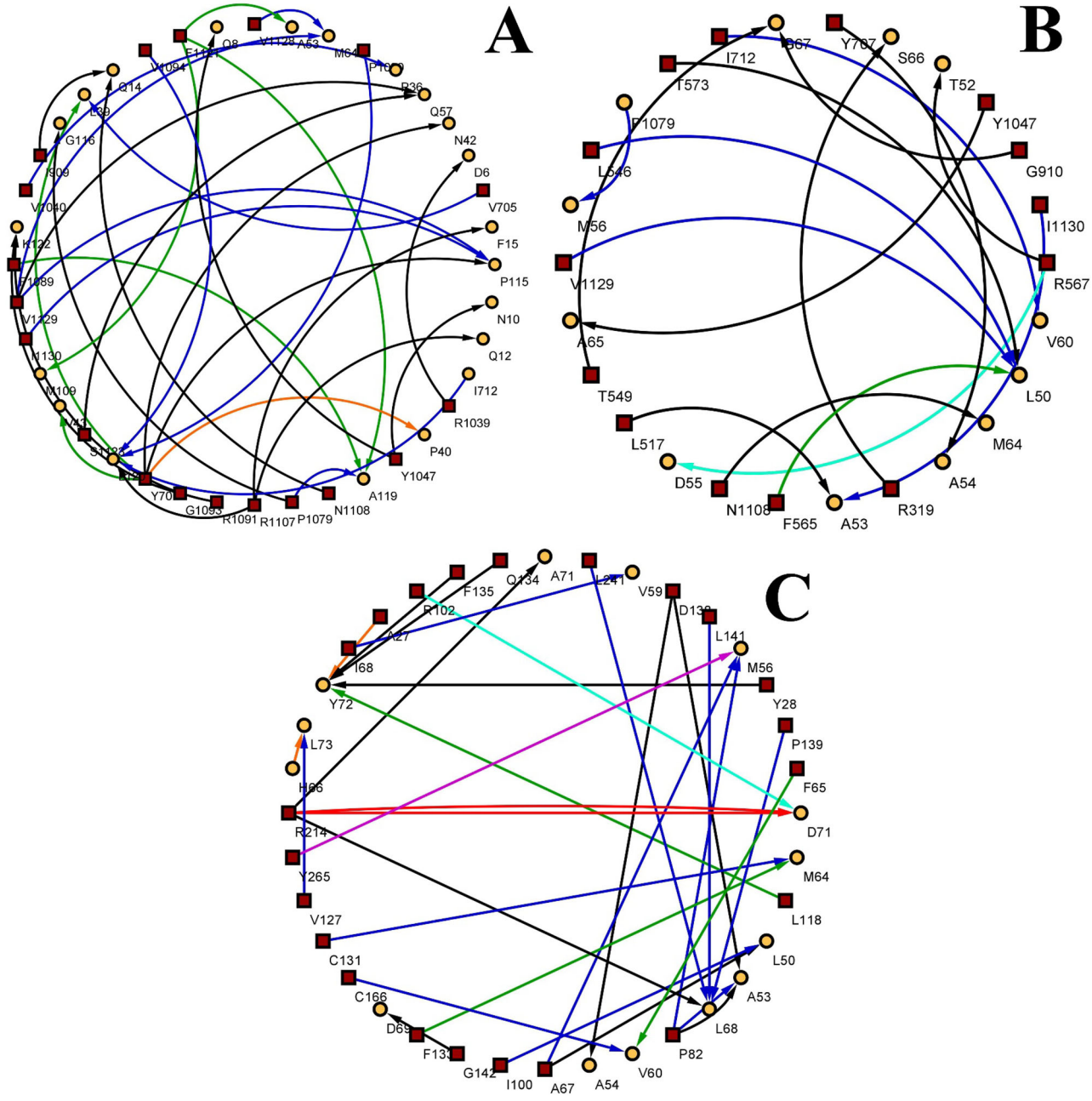

Figure 7. **Residue interaction network between S-protein and azurin/p18/p28:** As observed, azurin interacted better to the S2 domain of the spike protein, whereas the interaction between the S1 domain and the p18/p28 peptide were lesser. p28 interactions, even though relatively less, contained strong electrostatic and hydrogen bond formation. **(A)** Residue interactions between S-protein and azurin. **(B)** Residue interactions between S-protein and p18. **(C)** Residue interactions between S-protein and p28. S-protein is represented in brown square boxes, and docked molecules are shown in yellow circles. Interactions are colored based on their type: Alkyl (blue); Electrostatic (red); Hydrogen bond (black); pi-alkyl (green); pi-sigma (orange); pi-sulfur(magenta); salt bridges (cyan).

between ~0.18 nm to ~0.31 nm in the event of 60 ns of the timescale. Here, the p28 peptide adapts well inside the spike binding pocket, followed by conformational changes, which can be observed in the deviation peak near the 19th ns, and from there, the conformational stability occurs within the binding pocket and is stable throughout the MD simulations. In the human host, the ACE-2 and spike protein interact with each other to facilitate the entry of the virus, and this interaction of p28 peptide with ACE-2 and S-protein gives a possibility of p28 being a protein-protein interaction inhibitor. To understand the protein-peptide interactions and its energy levels in the 60 ns of MD simulations, statistical analysis along with prime MM/PBSA calculations of each 20 ns interval was calculated.

From the 60 ns of MD simulations, each 20 ns of intervals RMSD values were separated and analyzed for the determination of p28 binding behavior with 3CL^{pro}, PL^{pro}, S-protein, and ACE-2 proteins. For the ACE-2 protein, the whole RMSD plot shows stable positioning and the same seen in the statistical values. The average and mean values that lay between 0.27 to 0.29 showed similar pose binding of p28 with ACE-2 in 0–20th ns, 20th-40th ns, and 40th-60th ns. But for 3CL^{pro}, PL^{pro}, S-protein complexes with p28, the deviation interval seems to be higher, as shown in Table 1. This may be due to

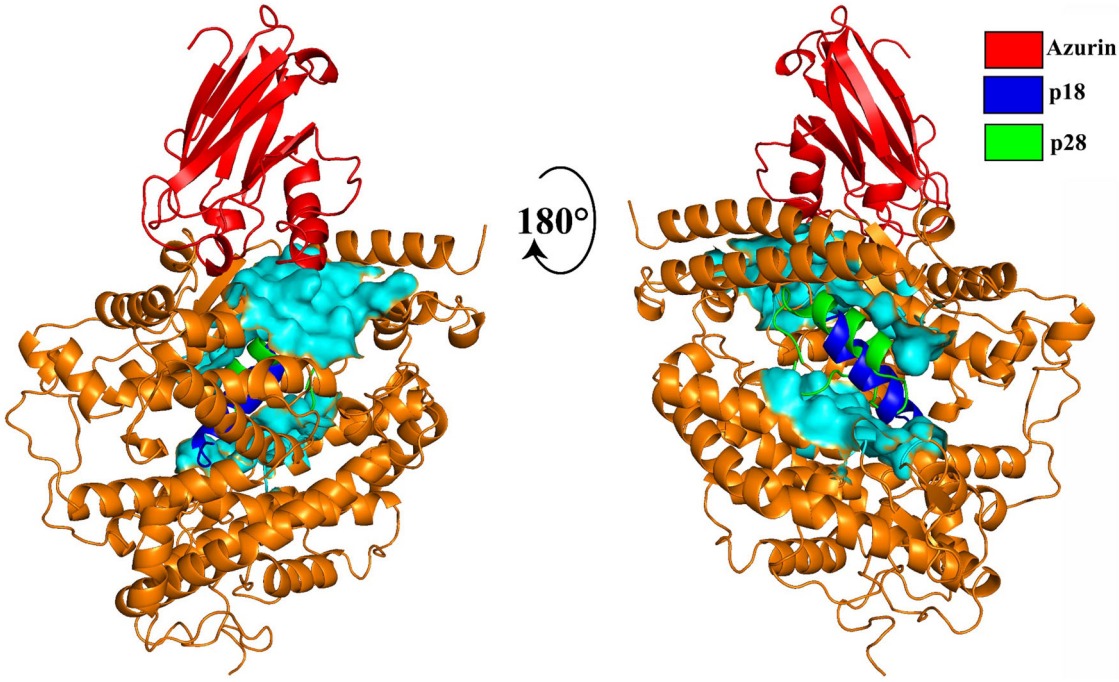

Figure 8. **Docking of azurin and its peptides to ACE-2:** ACE-2 is represented in orange while the surface of the binding site is in cyan. Azurin (red) was observed to bind to the collectrin domain of the ACE-2 receptor, while p18 and p28 can be seen binding to the active peptidase domain of the ACE-2 receptor.

the possibility of p28 binding in multiple conformations with $3CL^{pro}$, PL^{pro}, and S-protein and also supports active binding of p28. Overall statistical values of mean, median, and mode also lay in a similar way, which proves that the p28 binding could be approximately symmetrical. The values of the standard deviations are equal to the value of zero, which indicates the identical data seen in p28 interactions with the $3CL^{pro}$, PL^{pro}, S-protein, and ACE-2 proteins. Along with the statistical analysis of 20 ns intervals, these same intervals were subjected to binding energy calculations with MM/PBSA analysis. For ACE-2 bound with p28, the highest binding energy was valued between −125.609 to −138.512 kJ/mol, which is lower than the other three protein complexes. For $3CL^{pro}$, the binding energy was calculated to be between −183.970 to −192.354 kJ/mol. PL^{pro} with p28 complex had a binding energy value between the −160.023 to −181.338 kJ/mol. In comparison with ACE-2, $3CL^{pro,}$ and PL^{pro}, the S-protein complex to p28 exhibited strong binding energy with the values lies between the −206.898 to −238.222 KJ/mol. Overall, the energy profiles conclude that p28 bound moderately with ACE-2, and strongly with the S-protein. It can also be assumed that p28 might have a potential role as a protein-protein interaction inhibitor.

5. Discussion

The current SARS-CoV-2 pandemic has made the scientific world realize the shortage of options available to treat such neglected diseases. Even though the outbreak of SARS and MERS-CoV had claimed numerous lives, currently, there is no treatment or prevention protocol available against this group of viruses. Considering the need for a treatment, we conceived this study to assess the potential of azurin as an anti-SARS-CoV-2 agent. There have been previous attempts to develop inhibitors against the $3CL^{pro}$, PL^{pro}, spike protein, and other viral protein but most of them were small size molecules (Aanouz et al., 2020; Elfiky 2020a; 2020b; Joshi et al., 2020; Umesh et al., 2020). Before testing for *in vitro* and *in vivo*, it is necessary to establish the affinity of azurin and its peptides: p18 and p28 towards the key viral proteins. The study concentrated on targeting the viral non-structural proteins: $3CL^{pro}$ and PL^{pro} and the structural S-protein. Curious to determine if there is an affinity towards the ACE-2 receptor, we also analyzed the interaction between ACE-2 and azurin along with its peptide.

Azurin, produced by the pathogenic bacterium *Pseudomonas aeruginosa*, is a well-characterized member of the cupredoxin family. Several studies have shown that bacterial cupredoxins, particularly azurin, can serve as a source for the development of emerging therapeutic drugs to treat cancer as well as against various infectious agents, such as viruses (HIV) and parasites (*Plasmodium falciparum* and *Toxoplasma gondii*) (Chaudhari et al., 2006; Naguleswaran et al., 2008). Therefore, considering the therapeutic history of the protein, we docked it against the SARS-CoV-2 proteins to identify its affinity and study the interactions in detail. Azurin, when docked against $3CL^{pro}$ bound to the C terminal domain III of $3CL^{pro}$. Interestingly, this region of the main protease has been reported to be responsible for functional dimerization (Shi et al., 2004; Zhong et al., 2008). Azurin bound with good affinity to domain III of the main protease forming several favorable hydrogen bonds and salt bridges. In PL^{pro}, the catalytic triad was identified as C112-H273-S287 and the azurin bound to the ubiquitin-like domain (UBL) of the protease. The UBL is responsible in deubiquitination and deISGylation modifications in the virus and removal of N-terminal UBL led to a 6-fold loss in recognition of ISG-15 (Interferon-stimulated gene) (Báez-Santos et al., 2015; Lindner

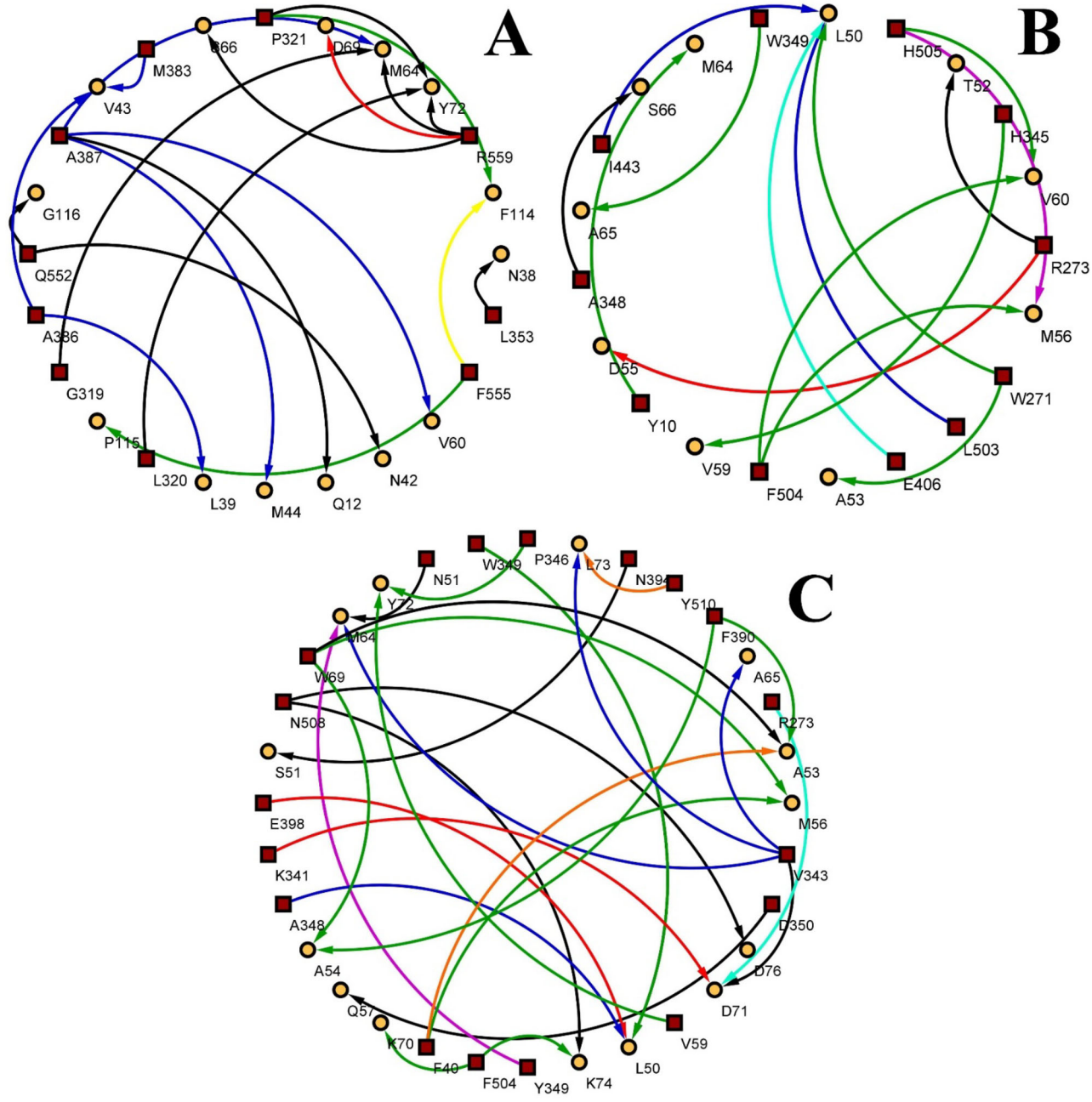

Figure 9. **Residue interaction network between ACE-2 and azurin/p18/p28:** Azurin and p18 interacted relatively lesser when compared with p28 interaction. p28, as seen in figure 8, binds to the peptidase domain of the ACE-2 receptor. **(A)** Residue interactions between ACE-2and azurin. **(B)** Residue interactions between ACE-2and p18. **(C)** Residue interactions between ACE-2and p28. ACE-2 is represented in brown square boxes, and docked molecules are shown in yellow circles. Alkyl (blue); Electrostatic (red); Hydrogen bond (black); pi-alkyl (green); pi-sigma (orange); pi-sulfur(magenta); pi-pi (yellow); salt bridges (cyan).

et al., 2005; Ratia et al., 2014). Binding of azurin to the UBL domain can lead to the inhibition of deubiquitination and deISGylation, thereby helping the host in mounting an ISG-mediated immune response. Azurin exhibited a strong binding affinity towards the S2 domain of the S-protein. We hypothesize that the binding of azurin to the S2 domain of the S-protein will help prevent the fusion of the virus as S2 is responsible for fusion with target cells. The binding to ACE-2 protein was relatively less when compared to the viral protein interactions.

The peptide fragment p18 (L50–G67) has been extracted from azurin peptide, and several anti-activities have been established earlier. Moreover, the administration of a small therapeutic peptide is always structurally better than the complete protein. Based on this, the p18 peptide was docked to the viral proteins. In $3CL^{pro}$, p18 also docked to the domain III of $3CL^{pro}$, but the interactions were lesser as compared to azurin. p18 bound to the active site of the PL^{pro} and interacted with the active site residues C111 and H272. The other interactions between p28 and the protease provided an idea on the high binding affinity when compared to $3CL^{pro}$ interaction. With S-protein, the interaction was observed in the critical S1 (N-terminal) domain, which houses the RBD (Du et al., 2009; Walls et al., 2020). The RBD helps the initial attachment of the virus to the ACE-2 receptor. Even though the binding was recorded, the interactions

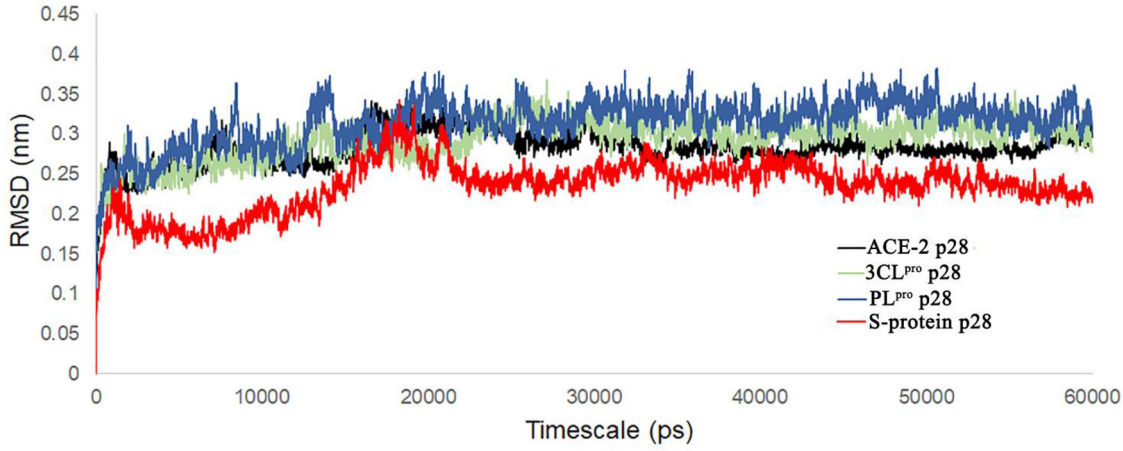

Figure 10. RMSD values of p28 peptide complexed with $3CL^{pro}$ (green), PL^{pro} (blue), S-protein (red), and ACE-2 (black) proteins plotted for the timescale of 60 ns through MD simulations.

Table 1. Statistical analysis of RMSD values for the 60 ns of MD simulations along with the MM/PBSA applied binding energy calculations.

Peptide Complex	Time	Mean	Median	Mode	Standard Deviation	Co-efficient of Variation	Binding energy (kJ/mol)
ACE-2 p28	0 ns – 20 ns	0.27161	0.26631	0.25685	0.02958	0.10891	−138.512 ± 24.071
$3CL^{pro}$ p28		0.26778	0.2706	0.25019	0.02418	0.09031	−192.354 ± 38.973
PL^{pro} p28		0.29021	0.29024	0.29418	0.03352	0.11549	−169.503 ± 31.651
S-protein p28		0.2135	0.20216	0.20105	0.04417	0.20687	−211.338 ± 27.633
ACE p28	20 ns – 40 ns	0.29365	0.29138	0.28256	0.01512	0.0515	−132.663 ± 23.380
$3CL^{pro}$ p28		0.30749	0.3087	0.28487	0.01673	0.05442	−189.109 ± 20.659
PL^{pro} p28		0.32589	0.32522	0.31878	0.01605	0.04925	−181.338 ± 35.518
S-protein p28		0.25060	0.24909	0.24506	0.01432	0.05715	−206.898 ± 21.683
ACE p28	40 ns – 60 ns	0.28283	0.28182	0.27255	0.00868	0.03071	−125.609 ± 18.692
$3CL^{pro}$ p28		0.30603	0.30614	0.29606	0.01176	0.03843	−183.970 ± 42.880
PL^{pro} p28		0.32791	0.32719	0.32806	0.01613	0.04918	−160.023 ± 33.681
S-protein p28		0.24125	0.23911	0.23044	0.01427	0.05916	−238.222 ± 38.571

between the residues of the complex suggested a relatively weak binding. The ACE-2 receptor binding, surprisingly, exhibited the p18 bound to the N-terminal domain of the ACE-2 receptor, which is the region where the RBD region of the spike protein binds to (Lan et al., 2020). But the residue interaction network (RIN) suggested a relatively low affinity and bond formation between the active peptidase domain and the p18 peptide.

Azurin showed good binding to all the proteins except with p18. Considering the results, we were curious to check if the anti-cancer peptide from azurin, i.e. p28 (L50 and D77), was capable of better binding to the viral proteins. Also, we wanted to know if the p28 peptide could interact with the ACE-2 receptor and block the binding of the S1 domain of SARS-CoV-2 S-protein. Docking results of $3CL^{pro}$ was similar to the azurin and p18, wherein the peptide interacted with the domain III residues. But, despite sharing the same binding site, p28 peptide formed a higher number of bonds with the amino acids of domain III. With PL^{pro}, p28 bound to the finger domain of the papain-like protease. The finger domain in PL^{pro} houses a zinc ion that forms coordination with four cysteine residues in a tetrahedral manner. This function is critical for the catalysis of PL^{pro} and also to maintain structural integrity (Barretto et al., 2005; Ratia et al., 2014). The RIN corroborated the strong binding affinity of the p28 peptide to the finger domain of the PL^{pro}. Once the affinity of p28 to the non-structural proteins was established, we checked for structural protein attraction. Like p18, p28 also bound to the S1 domain of the S-protein, but in the C-terminal. Another difference observed was the better bond formation (both in terms of hydrogen bonds and electrostatic interactions) of p28 in comparison to p18 peptide. The binding pattern of p28 to ACE-2 was also identical, sharing the same binding pocket, but as observed in the S-protein docking, p28 outsmarted p18 from the stability point of view. The peptide fragment p28 stabilized itself in the ACE-2 receptor by forming hydrogen bonds, electrostatic as well as alkyl interactions. Drawing from the results, we hypothesized that the peptide fragment p28 has better potential as an antiviral against SARS-Cov-2 than the whole protein azurin and the peptide fragment p18. To further fortify the findings of p28 affinity, we simulated the p28 complexed with $3CL^{pro}$, PL^{pro}, S-protein, and ACE-2 receptor for a period of 60 ns. The RMSD of the complexes were stable throughout the 60 ns time period, indicating that the p28 peptide complexed well with the viral protein and the ACE-2 receptor at the binding site. Further statistical analysis and MM/PBSA analysis led us to discover the p28 had a high affinity to S-protein and moderately towards the ACE-2 receptor. Results from previous studies have shown RMSD values as seen in this study being stable in nature (Bohra et al., 2020; Mittal et al., 2020; Shukla et al., 2018; et al., 2018). The energy calculations with $3CL^{pro}$

and PL^{pro} were relatively low when compared to former proteins. This led us to hypothesize that p28 could be a potent inhibitor of the ACE-2-S-protein interaction that is responsible for the viral invasion mechanism od SARS-CoV-2. But also, considering the affinity of p28 towards $3CL^{pro}$ as the second highest, there is a possibility that p28 binds to $3CL^{pro}$ too.

The study, in a nutshell, was focused on identifying if azurin and its peptides were capable to promote functional inhibition of molecular/cellular events relevant for SARS-CoV-2 infection. Among the studied azurin protein and its peptides, we believe that p28 might exhibit better activity, and previous reports corroborate the statement. This study, though primary, would require extensive *in vitro* and *in vivo* studies before the hypothesized p28 activity can be established. Moreover, given the previous reports of azurin and its peptide exhibiting anti-HIV activity, p28 might be the therapeutic drug that is essential for the current crisis. The p28 peptide, if found active, can be helpful in the treatment of current SARS-CoV-2 burden and also prevent future infections from this group of viruses.

Acknowledgements

The author SS acknowledges research fellowship from NIT Warangal. CS and SKS thankfully acknowledge RUSA-Phase 2.0 Policy (TNmulti-Gen), Dept. of Edn, Govt. of India (Grant No: F.24-51/2014-U).

Disclosure statement

No potential conflict of interest is reported by the authors.

Funding

No funding was availed for this study.

Author contribution

Santanu Sasidharan: Methodology, Software, Validation and Writing-initial draft preparation. Chandrabose Selvaraj: Software, Validation, Writing-Reviewing and Editing; Sanjeev Kumar Singh: Software, Visualization, Validation, Writing-Reviewing and Editing; Vikash Kumar Dubey: Software, Writing-Reviewing and Editing; Sachin Kumar: Conceptualization, Writing-Reviewing and Editing; Arsénio M Fialho: Conceptualization, Resources, Writing-Reviewing and Editing; Prakash Saudagar: Conceptualization, Visualization, Validation, Supervision, Project administration, Writing-Reviewing, and Editing. All authors contributed their inputs in the writing of the draft.

ORCID

Santanu Sasidharan http://orcid.org/0000-0002-0204-0263
Chandrabose Selvaraj http://orcid.org/0000-0002-8115-0486
Sachin Kumar http://orcid.org/0000-0002-8526-6013
Arsenio M. Fialho http://orcid.org/0000-0002-8066-5787
Prakash Saudagar http://orcid.org/0000-0001-7211-0581

References

Aanouz, I., Belhassan, A., Khatabi, K. E., Lakhlifi, T., Idrissi, M. E., & Bouachrine, M. (2020). Moroccan Medicinal plants as inhibitors of COVID-19: Computational investigations. *Journal of Biomolecular Structure and Dynamics*, *38*, 1–12.

Abdelli, I., Hassani, F., Bekkel Brikci, S., & Ghalem, S. (2020). In silico study the inhibition of Angiotensin converting enzyme 2 receptor of COVID-19 by Ammoides verticillata components harvested from western Algeria. *Journal of Biomolecular Structure and Dynamics*, *38*, 1–17. https://doi.org/10.1080/07391102.2020.1763199

Al-Khafaji, K., Al-DuhaidahawiL, D., & Taskin Tok, T. (2020). Using integrated computational approaches to identify safe and rapid treatment for SARS-CoV-2. *Journal of Biomolecular Structure and Dynamics*, *38*, 1–11. https://doi.org/10.1080/07391102.2020.1764392

Báez-Santos, Y. M., John, S. E. S., & Mesecar, A. D. (2015). The SARS-coronavirus papain-like protease: Structure, function and inhibition by designed antiviral compounds. *Antiviral Research*, *115*, 21–38. https://doi.org/10.1016/j.antiviral.2014.12.015

Barretto, N., Jukneliene, D., Ratia, K., Chen, Z., Mesecar, A. D., & Baker, S. C. (2005). The papain-like protease of severe acute respiratory syndrome coronavirus has deubiquitinating activity. *Journal of Virology*, *79*(24), 15189–15198. https://doi.org/10.1128/JVI.79.24.15189-15198.2005

Bohra, N., Sasidharan, S., Raj, S., Balaji, S., & Saudagar, P. (2020). Utilising capsid proteins of poliovirus to design a multi-epitope based subunit vaccine by immunoinformatics approach. *Molecular Simulation*, *46*(5), 419–428. https://doi.org/10.1080/08927022.2020.1720916

Boopathi, S., Poma, A. B., & Kolandaivel, P. (2020). Novel 2019 Coronavirus Structure, Mechanism of Action, Antiviral drug promises and rule out against its treatment. *Journal of Biomolecular Structure and Dynamics*, *38*, 1–14. https://doi.org/10.1080/07391102.2020.1758788

Bosch, B. J., van der Zee, R., de Haan, C. A., & Rottier, P. J. (2003). The coronavirus spike protein is a class I virus fusion protein: Structural and functional characterization of the fusion core complex. *Journal of Virology*, *77*(16), 8801–8811. https://doi.org/10.1128/jvi.77.16.8801-8811.2003

Chakrabarty, A. M. (2016). Bacterial azurin in potential cancer therapy. *Cell Cycle (Georgetown, Tex.)*, *15*(13), 1665–1666. https://doi.org/10.1080/15384101.2016.1179034

Chan, J. F. W., Chan, K.-H., Kao, R. Y. T., To, K. K. W., Zheng, B.-J., Li, C. P. Y., Li, P. T. W., Dai, J., Mok, F. K. Y., Chen, H., Hayden, F. G., & Yuen, K.-Y. (2013). Broad-spectrum antivirals for the emerging Middle East respiratory syndrome coronavirus. *The Journal of Infection*, *67*(6), 606–616. https://doi.org/10.1016/j.jinf.2013.09.029

Chaudhari, A., Fialho, A. M., Ratner, D., Gupta, P., Hong, C. S., Kahali, S., Yamada, T., Haldar, K., Murphy, S., Cho, W., Chauhan, V. S., Das Gupta, T. K., & Chakrabarty, A. M. (2006). Azurin, Plasmodium falciparum malaria and HIV/AIDS: Inhibition of parasitic and viral growth by Azurin. *Cell Cycle (Georgetown, Tex.).)*, *5*(15), 1642–1648. https://doi.org/10.4161/cc.5.15.2992

Cheng, V. C., Lau, S. K., Woo, P. C., & Yuen, K. Y. (2007). Severe acute respiratory syndrome coronavirus as an agent of emerging and reemerging infection. *Clinical Microbiology Reviews*, *20*(4), 660–694. https://doi.org/10.1128/CMR.00023-07

Chen, Y., Liu, Q., & Guo, D. (2020). Emerging coronaviruses: Genome structure, replication, and pathogenesis. *Journal of Medical Virology*, *92*(4), 418–423. https://doi.org/10.1002/jmv.25681

Chen, X., Yang, X., Zheng, Y., Yang, Y., Xing, Y., & Chen, Z. (2014). SARS coronavirus papain-like protease inhibits the type I interferon signaling pathway through interaction with the STING-TRAF3-TBK1 complex. *Protein & Cell*, *5*(5), 369–381. https://doi.org/10.1007/s13238-014-0026-3

Chen, N., Zhou, M., Dong, X., Qu, J., Gong, F., Han, Y., Qiu, Y., Wang, J., Liu, Y., Wei, Y., Xia, J., Yu, T., Zhang, X., & Zhang, L. (2020). Epidemiological and clinical characteristics of 99 cases of 2019 novel coronavirus pneumonia in Wuhan, China: A descriptive study. *The Lancet*, *395*(10223), 507–513. https://doi.org/10.1016/S0140-6736(20)30211-7

Chinnasamy, S., Selvaraj, G., Kaushik, A. C., Kaliamurthi, S., Chandrabose, S., Singh, S. K., Thirugnanasambandam, R., Gu, K., & Wei, D. Q. (2019). Molecular docking and molecular dynamics simulation studies to identify potent AURKA inhibitors: Assessing the performance of density functional theory, MM-GBSA and mass action kinetics calculations. *Journal of Biomolecular Structure and Dynamics*, *37*, 1–11. https://doi.org/10.1080/07391102.2019.1674695

Chinnasamy, S., Selvaraj, G., Selvaraj, C., Kaushik, A. C., Kaliamurthi, S., Khan, A., Singh, S. K., & Wei, D. Q. (2020). Combining in silico and in vitro

approaches to identification of potent inhibitor against phospholipase A2 (PLA2). *International Journal of Biological Macromolecules*, *144*, 53–66. https://doi.org/10.1016/j.ijbiomac.2019.12.091

Das, S., Sarmah, S., Lyndem, S., & Singha Roy, A. (2020). An investigation into the identification of potential inhibitors of SARS-CoV-2 main protease using molecular docking study. *Journal of Biomolecular Structure and Dynamics*, *38*, 1–18.

de Groot, R. J., Baker, S. C., Baric, R. S., Brown, C. S., Drosten, C., Enjuanes, L., Fouchier, R. A. M., Galiano, M., Gorbalenya, A. E., Memish, Z. A., Perlman, S., Poon, L. L. M., Snijder, E. J., Stephens, G. M., Woo, P. C. Y., Zaki, A. M., Zambon, M., & Ziebuhr, J. (2013). Commentary: Middle East respiratory syndrome coronavirus (MERS-CoV): Announcement of the Coronavirus Study Group. *Journal of Virology*, *87*(14), 7790–7792. https://doi.org/10.1128/JVI.01244-13

de Wilde, A. H., Jochmans, D., Posthuma, C. C., Zevenhoven-Dobbe, J. C., van Nieuwkoop, S., Bestebroer, T. M., van den Hoogen, B. G., Neyts, J., & Snijder, E. J. (2014). Screening of an FDA-approved compound library identifies four small-molecule inhibitors of Middle East respiratory syndrome coronavirus replication in cell culture. *Antimicrobial Agents and Chemotherapy*, *58*(8), 4875–4884. https://doi.org/10.1128/AAC.03011-14

Du, L., He, Y., Zhou, Y., Liu, S., Zheng, B.-J., & Jiang, S. (2009). The spike protein of SARS-CoV-a target for vaccine and therapeutic development. *Nature Reviews. Microbiology*, *7*(3), 226–236. https://doi.org/10.1038/nrmicro2090

Duncan, A. L., Robinson, A. J., & Walker, J. E. (2016). Cardiolipin binds selectively but transiently to conserved lysine residues in the rotor of metazoan ATP synthases. *Proceedings of the National Academy of Sciences of the United States of America*, *113*(31), 8687–8692. https://doi.org/10.1073/pnas.1608396113

Dyall, J., Coleman, C. M., Hart, B. J., Venkataraman, T., Holbrook, M. R., Kindrachuk, J., Johnson, R. F., Olinger, G. G., Jahrling, P. B., Laidlaw, M., Johansen, L. M., Lear-Rooney, C. M., Glass, P. J., Hensley, L. E., & Frieman, M. B. (2014). Repurposing of clinically developed drugs for treatment of Middle East respiratory syndrome coronavirus infection. *Antimicrobial Agents and Chemotherapy*, *58*(8), 4885–4893. https://doi.org/10.1128/AAC.03036-14

Elfiky, A. A. (2020a). Natural products may interfere with SARS-CoV-2 attachment to the host cell. *Journal of Biomolecular Structure and Dynamics*, *38*, 1–16.

Elfiky, A. A. (2020b). SARS-CoV-2 RNA dependent RNA polymerase (RdRp) targeting: An in silico perspective. *Journal of Biomolecular Structure and Dynamics*, *38*, 1–15.

Elfiky, A. A., & Azzam, E. B. (2020). Novel Guanosine Derivatives against MERS CoV polymerase: An in silico perspective. *Journal of Biomolecular Structure and Dynamics*, *38*, 1–12.

Elmezayen, A. D., Al-Obaidi, A., Şahin, A. T., & Yelekçi, K. (2020). Drug repurposing for coronavirus (COVID-19): In silico screening of known drugs against coronavirus 3CL hydrolase and protease enzymes. *Journal of Biomolecular Structure and Dynamics*, *38*, 1–12.

Enayatkhani, M., Hasaniazad, M., Faezi, S., Guklani, H., Davoodian, P., Ahmadi, N., Einakian, M. A., Karmostaji, A., & Ahmadi, K. (2020). Reverse vaccinology approach to design a novel multi-epitope vaccine candidate against COVID-19: An in silico study. *Journal of Biomolecular Structure and Dynamics*, *38*, 1–19.

Garzon, J. I., Lopéz-Blanco, J. R., Pons, C., Kovacs, J., Abagyan, R., Fernandez-Recio, J., & Chacon, P. (2009). FRODOCK: A new approach for fast rotational protein-protein docking. *Bioinformatics (Oxford, England)*, *25*(19), 2544–2551. https://doi.org/10.1093/bioinformatics/btp447

Gupta, M. K., Vemula, S., Donde, R., Gouda, G., Behera, L., & Vadde, R. (2020). In-silico approaches to detect inhibitors of the human severe acute respiratory syndrome coronavirus envelope protein ion channel. *Journal of Biomolecular Structure and Dynamics*, *38*, 1–11.

Gyebi, G. A., Ogunro, O. B., Adegunloye, A. P., Ogunyemi, O. M., & Afolabi, S. O. (2020). Potential inhibitors of coronavirus 3-chymotrypsin-like protease (3CLpro): An in silico screening of alkaloids and terpenoids from African medicinal plants. *Journal of Biomolecular Structure and Dynamics*, *38*, 1–19.

Habault, J., & Poyet, J.-L. (2019). Recent advances in cell penetrating peptide-based anticancer therapies. *Molecules*, *24*(5), 927. https://doi.org/10.3390/molecules24050927

Harcourt, B. H., Jukneliene, D., Kanjanahaluethai, A., Bechill, J., Severson, K. M., Smith, C. M., Rota, P. A., & Baker, S. C. (2004). Identification of severe acute respiratory syndrome coronavirus replicase products and characterization of papain-like protease activity. *Journal of Virology*, *78*(24), 13600–13612. https://doi.org/10.1128/JVI.78.24.13600-13612.2004

Hasan, A., Paray, B. A., Hussain, A., Qadir, F. A., Attar, F., Aziz, F. M., Sharifi, M., Derakhshankhah, H., Rasti, B., & Mehrabi, M. (2020). A review on the cleavage priming of the spike protein on coronavirus by angiotensin-converting enzyme-2 and furin. *Journal of Biomolecular Structure and Dynamics*, *38*, 1–13.

Hoffmann, M., Kleine-Weber, H., Krüger, N., Mueller, M. A., Drosten, C., & Pöhlmann, S. (2020). The novel coronavirus 2019 (2019-nCoV) uses the SARS-coronavirus receptor ACE2 and the cellular protease TMPRSS2 for entry into target cells. *BioRxiv*, 1–23.

Huang, C., Wang, Y., Li, X., Ren, L., Zhao, J., Hu, Y., Zhang, L., Fan, G., Xu, J., Gu, X., Cheng, Z., Yu, T., Xia, J., Wei, Y., Wu, W., Xie, X., Yin, W., Li, H., Liu, M. … Cao, B. (2020). Clinical features of patients infected with 2019 novel coronavirus in Wuhan, China. *The Lancet* , *395*(10223), 497–506. https://doi.org/10.1016/S0140-6736(20)30183-5

Islam, R., Parves, R., Paul, A. S., Uddin, N., Rahman, M. S., Mamun, A. A., Hossain, M. N., Ali, M. A., & Halim, M. A. (2020). A molecular modeling approach to identify effective antiviral phytochemicals against the main protease of SARS-CoV-2. *Journal of Biomolecular Structure and Dynamics*, *38*, 1–20.

Joshi, R. S., Jagdale, S. S., Bansode, S. B., Shankar, S. S., Tellis, M. B., Pandya, V. K., Chugh, A., Giri, A. P., & Kulkarni, M. J. (2020). Discovery of Potential Multi-Target-Directed Ligands by Targeting Host-specific SARS-CoV-2 Structurally Conserved Main Protease$. *Journal of Biomolecular Structure and Dynamics*, *38*, 1–16.

Kalita, P., Lyngdoh, D. L., Padhi, A. K., Shukla, H., & Tripathi, T. (2019). Development of multi-epitope driven subunit vaccine against Fasciola gigantica using immunoinformatics approach. *International Journal of Biological Macromolecules*, *138*, 224–233. https://doi.org/10.1016/j.ijbiomac.2019.07.024

Kalita, P., Padhi, A., Zhang, K. Y., & Tripathi, T. (2020). Design of a peptide-based subunit vaccine against novel coronavirus SARS-CoV-2. *Microbial Pathogenesis*, *145*, 104236. https://doi.org/10.1016/j.micpath.2020.104236

Khan, R. J., Jha, R. K., Amera, G. M., Jain, M., Singh, E., Pathak, A., Singh, R. P., Muthukumaran, J., & Singh, A. K. (2020). Targeting SARS-CoV-2: A systematic drug repurposing approach to identify promising inhibitors against 3C-like proteinase and 2′-O-ribose methyltransferase. *Journal of Biomolecular Structure and Dynamics*, *38*, 1–14.

Khan, S. A., Zia, K., Ashraf, S., Uddin, R., & Ul-Haq, Z. (2020). Identification of chymotrypsin-like protease inhibitors of SARS-CoV-2 via integrated computational approach. *Journal of Biomolecular Structure and Dynamics*, *38*, 1–10.

Kozakov, D., Hall, D. R., Xia, B., Porter, K. A., Padhorny, D., Yueh, C., Beglov, D., & Vajda, S. (2017). The ClusPro web server for protein–protein docking. *Nature Protocols*, *12*(2), 255–278. https://doi.org/10.1038/nprot.2016.169

Kumar, D., Kumari, K., Jayaraj, A., Kumar, V., Kumar, R. V., Dass, S. K., Chandra, R., & Singh, P. (2020). Understanding the binding affinity of noscapines with protease of SARS-CoV-2 for COVID-19 using MD simulations at different temperatures. *Journal of Biomolecular Structure and Dynamics*, *38*, 1–14.

Kumari, R., Kumar, R., & A. Lynn, (2014). g_mmpbsa-a GROMACS tool for high-throughput MM-PBSA calculations . *Journal of Chemical Information and Modeling*, *54*(7), 1951–1962. https://doi.org/10.1021/ci500020m

Lan, J., Ge, J., Yu, J., Shan, S., Zhou, H., Fan, S., Zhang, Q., Shi, X., Wang, Q., & Zhang, L. (2020). Structure of the SARS-CoV-2 spike receptor-binding domain bound to the ACE2 receptor. *Nature*, *581*(7807), 1–9.

Lau, S. K., Woo, P. C., Li, K. S., Huang, Y., Tsoi, H.-W., Wong, B. H., Wong, S. S., Leung, S.-Y., Chan, K.-H., & Yuen, K.-Y. (2005). Severe acute respiratory syndrome coronavirus-like virus in Chinese horseshoe bats. *Proceedings of*

the National Academy of Sciences of the United States of America, *102*(39), 14040–14045. https://doi.org/10.1073/pnas.0506735102

Lee, N., Hui, D., Wu, A., Chan, P., Cameron, P., Joynt, G. M., Ahuja, A., Yung, M. Y., Leung, C. B., To, K. F., Lui, S. F., Szeto, C. C., Chung, S., & Sung, J. J. Y. (2003). A major outbreak of severe acute respiratory syndrome in Hong Kong. *New England Journal of Medicine*, *348*(20), 1986–1994. https://doi.org/10.1056/NEJMoa030685

Li, S.-W., Wang, C.-Y., Jou, Y.-J., Huang, S.-H., Hsiao, L.-H., Wan, L., Lin, Y.-J., Kung, S.-H., & Lin, C.-W. (2016). SARS coronavirus papain-like protease inhibits the TLR7 signaling pathway through removing Lys63-linked polyubiquitination of TRAF3 and TRAF6. *International Journal of Molecular Sciences*, *17*(5), 678. https://doi.org/10.3390/ijms17050678

Lindner, H. A., Fotouhi-Ardakani, N., Lytvyn, V., Lachance, P., Sulea, T., & Ménard, R. (2005). The papain-like protease from the severe acute respiratory syndrome coronavirus is a deubiquitinating enzyme. *Journal of Virology*, *79*(24), 15199–15208. https://doi.org/10.1128/JVI.79.24.15199-15208.2005

Lobo-Galo, N., Terrazas-López, M., Martínez-Martínez, A., & Díaz-Sánchez, Á. G. (2020). FDA-approved thiol-reacting drugs that potentially bind into the SARS-CoV-2 main protease, essential for viral replication. *Journal of Biomolecular Structure and Dynamics*, *38*, 1–12.

Mittal, A., Sasidharan, S., Raj, S., Balaji, S., & Saudagar, P. (2020). Exploring the Zika Genome to Design a Potential Multiepitope Vaccine Using an Immunoinformatics Approach. *International Journal of Peptide Research and Therapeutics*, *26*, 1–10.

Muralidharan, N., Sakthivel, R., Velmurugan, D., & Gromiha, M. M. (2020). Computational studies of drug repurposing and synergism of lopinavir, oseltamivir and ritonavir binding with SARS-CoV-2 Protease against COVID-19. *Journal of Biomolecular Structure and Dynamics*, *38*, 1–6.

Naguleswaran, A., Fialho, A. M., Chaudhari, A., Hong, C. S., Chakrabarty, A. M., & Sullivan, W. J. (2008). Azurin-like protein blocks invasion of Toxoplasma gondii through potential interactions with parasite surface antigen SAG1. *Antimicrobial Agents and Chemotherapy*, *52*(2), 402–408. https://doi.org/10.1128/AAC.01005-07

Nava, M. (2018). Implementing dimer metadynamics using gromacs. *Journal of Computational Chemistry*, *39*(25), 2126–2132. https://doi.org/10.1002/jcc.25386

Omrani, A. S., Saad, M. M., Baig, K., Bahloul, A., Abdul-Matin, M., Alaidaroos, A. Y., Almakhlafi, G. A., Albarrak, M. M., Memish, Z. A., & Albarrak, A. M. (2014). Ribavirin and interferon alfa-2a for severe Middle East respiratory syndrome coronavirus infection: A retrospective cohort study. *The Lancet Infectious Diseases*, *14*(11), 1090–1095. https://doi.org/10.1016/S1473-3099(14)70920-X

Padhi, A. K., Kalita, P., Zhang, K. Y., & Tripathi, T. (2020). High Throughput Designing and Mutational Mapping of RBD-ACE2 Interface Guide Non-Conventional Therapeutic Strategies for COVID-19. *bioRxiv*, 1–27.

Pant, S., Singh, M., Ravichandiran, V., Murty, U., & Srivastava, H. K. (2020). Peptide-like and small-molecule inhibitors against Covid-19. *Journal of Biomolecular Structure and Dynamics*, *38*, 1–15.

Pettersen, E. F., Goddard, T. D., Huang, C. C., Couch, G. S., Greenblatt, D. M., Meng, E. C., & Ferrin, T. E. (2004). UCSF Chimera-a visualization system for exploratory research and analysis. *Journal of Computational Chemistry*, *25*(13), 1605–1612. https://doi.org/10.1002/jcc.20084

Qi, R., Wei, G., Ma, B., & Nussinov, R. (2018). Replica Exchange Molecular Dynamics: A Practical Application Protocol with Solutions to Common Problems and a Peptide Aggregation and Self-Assembly Example. *Methods in Molecular Biology.*, *1777*, 101–119.

Ramírez-Aportela, E., López-Blanco, J. R., & Chacón, P. (2016). FRODOCK 2.0: Fast protein-protein docking server. *Bioinformatics (Oxford, England)*, *32*(15), 2386–2388. https://doi.org/10.1093/bioinformatics/btw141

Ratia, K., Kilianski, A., Baez-Santos, Y. M., Baker, S. C., & Mesecar, A. (2014). Structural basis for the ubiquitin-linkage specificity and deISGylating activity of SARS-CoV papain-like protease. *PLoS Pathogens*, *10*(5), e1004113. https://doi.org/10.1371/journal.ppat.1004113

Reusken, C. B., Haagmans, B. L., Müller, M. A., Gutierrez, C., Godeke, G.-J., Meyer, B., Muth, D., Raj, V. S., Vries, L. S.-D., Corman, V. M., Drexler, J.-F., Smits, S. L., El Tahir, Y. E., De Sousa, R., van Beek, J., Nowotny, N., van Maanen, K., Hidalgo-Hermoso, E., Bosch, B.-J. … Koopmans, M. P. G. (2013). Middle East respiratory syndrome coronavirus neutralising serum antibodies in dromedary camels: A comparative serological study. *The Lancet Infectious Diseases*, *13*(10), 859–866. https://doi.org/10.1016/S1473-3099(13)70164-6

Sarma, P., Shekhar, N., Prajapat, M., Avti, P., Kaur, H., Kumar, S., Singh, S., Kumar, H., Prakash, A., & Dhibar, D. P. (2020). In-silico homology assisted identification of inhibitor of RNA binding against 2019-nCoV N-protein (N terminal domain). *Journal of Biomolecular Structure and Dynamics*, *38*, 1–9.

Sasidharan, S., & Saudagar, P. (2019). Biochemical and structural characterization of tyrosine aminotransferase suggests broad substrate specificity and a two-state folding mechanism in Leishmania donovani . *FEBS Open Bio*, *9*(10), 1769–1783. https://doi.org/10.1002/2211-5463.12715

Sasidharan, S., & Saudagar, P. (2020). Concerted motion of structure and active site charge is required for tyrosine aminotransferase activity in Leishmania parasite. *Spectrochimica Acta. Part A, Molecular and Biomolecular Spectroscopy*, *232*, 118133https://doi.org/10.1016/j.saa.2020.118133

Selvaraj, C., Sakkiah, S., Tong, W., & Hong, H. (2018). Molecular dynamics simulations and applications in computational toxicology and nanotoxicology. Food Chem. Toxicol, *112*, 495–506. https://doi.org/10.1016/j.fct.2017.08.028

Selvaraj, C., Singh, P., & Singh, S. K. (2014). Investigations on the interactions of λphage-derived peptides against the SrtA mechanism in Bacillus anthracis . *Applied Biochemistry and Biotechnology*, *172*(4), 1790–1806. https://doi.org/10.1007/s12010-013-0641-0

Selvaraj, C., Singh, P., & Singh, S. K. (2014). Molecular insights on analogs of HIV PR inhibitors toward HTLV-1 PR through QM/MM interactions and molecular dynamics studies: Comparative structure analysis of wild and mutant HTLV-1 PR. *Journal of Molecular Recognition: JMR*, *27*(12), 696–706. https://doi.org/10.1002/jmr.2395

Shafique, S., & Rashid, S. (2019). Structural basis of βTrCP1-associated GLI3 processing . *Scientific Reports*, *9*(1), 6865https://doi.org/10.1038/s41598-019-43392-3

Shannon, P., Markiel, A., Ozier, O., Baliga, N. S., Wang, J. T., Ramage, D., Amin, N., Schwikowski, B., & Ideker, T. (2003). Cytoscape: A software environment for integrated models of biomolecular interaction networks. *Genome Research*, *13*(11), 2498–2504. https://doi.org/10.1101/gr.1239303

Shi, J., Wei, Z., & Song, J. (2004). Dissection Study on the Severe Acute Respiratory Syndrome 3C-like Protease reveals the critical role of the extra domain in dimerization of the enzyme: Defining the extra domain as a new target for design of highly specific protease inhibitors. *The Journal of Biological Chemistry*, *279*(23), 24765–24773. https://doi.org/10.1074/jbc.M311744200

Shukla, R., Chetri, P. B., Sonkar, A., Pakharukova, M. Y., Mordvinov, V. A., & Tripathi, T. (2018). Identification of novel natural inhibitors of Opisthorchis felineus cytochrome P450 using structure-based screening and molecular dynamic simulation. *Journal of Biomolecular Structure and Dynamics*, *36*(13), 3541–3556. https://doi.org/10.1080/07391102.2017.1392897

Shukla, R., Shukla, H., & Tripathi, T. (2020). Structure-based discovery of phenyl-diketo acids derivatives as Mycobacterium tuberculosis malate synthase inhibitors. *Journal of Biomolecular Structure and Dynamics*, *38*, 1–14.

Shukla, R., Shukla, H., Kalita, P., Sonkar, A., Pandey, T., Singh, D. B., Kumar, A., & Tripathi, T. (2018). Identification of potential inhibitors of Fasciola gigantica thioredoxin1: Computational screening, molecular dynamics simulation, and binding free energy studies. *Journal of Biomolecular Structure & Dynamics*, *36*(8), 2147–2162. https://doi.org/10.1080/07391102.2017.1344141

Sinha, S. K., Shakya, A., Prasad, S. K., Singh, S., Gurav, N. S., Prasad, R. S., & Gurav, S. S. (2020). An in-silico evaluation of different Saikosaponins for their potency against SARS-CoV-2 using NSP15 and fusion spike glycoprotein as targets. *Journal of Biomolecular Structure and Dynamics*, *38*, 1–13.

Tai, W., He, L., Zhang, X., Pu, J., Voronin, D., Jiang, S., Zhou, Y., & Du, L. (2020). Characterization of the receptor-binding domain (RBD) of 2019 novel coronavirus: Implication for development of RBD protein as a viral

attachment inhibitor and vaccine. *Cellular & Molecular Immunology*, *17*(6), 613–618. https://doi.org/10.1038/s41423-020-0400-4

Taylor, B. N., Mehta, R. R., Yamada, T., Lekmine, F., Christov, K., Chakrabarty, A. M., Green, A., Bratescu, L., Shilkaitis, A., Beattie, C. W., & Das Gupta, T. K. (2009). Noncationic peptides obtained from azurin preferentially enter cancer cells. *Cancer Research*, *69*(2), 537–546. https://doi.org/10.1158/0008-5472.CAN-08-2932

Umesh, Kundu, D., Selvaraj, C., Singh, S. K. & Dubey, V. K. (2020). Identification of new anti-nCoV drug chemical compounds from Indian spices exploiting SARS-CoV-2 main protease as target. *Journal of Biomolecular Structure and Dynamics*, *38*, 1–9.

Vajda, S., Yueh, C., Beglov, D., Bohnuud, T., Mottarella, S. E., Xia, B., Hall, D. R., & Kozakov, D. (2017). New additions to the ClusPro server motivated by CAPRI. *Proteins*, *85*(3), 435–444. https://doi.org/10.1002/prot.25219

Van Der Spoel, D., Lindahl, E., Hess, B., Groenhof, G., Mark, A. E., & Berendsen, H. J. (2005). GROMACS: Fast, flexible, and free. *Journal of Computational Chemistry*, *26*(16), 1701–1718. https://doi.org/10.1002/jcc.20291

Walls, A. C., Park, Y.-J., Tortorici, M. A., Wall, A., McGuire, A. T., & Veesler, D. (2020). Structure, function, and antigenicity of the SARS-CoV-2 spike glycoprotein. *Cell*, *181*(2), 281–292.e6. https://doi.org/10.1016/j.cell.2020.02.058

Wu, C., Liu, Y., Yang, Y., Zhang, P., Zhong, W., Wang, Y., Wang, Q., Xu, Y., Li, M., Li, X., Zheng, M., Chen, L., & Li, H. (2020). Analysis of therapeutic targets for SARS-CoV-2 and discovery of potential drugs by computational methods. *Acta Pharmaceutica Sinica B*, *10*(5), 766–788. https://doi.org/10.1016/j.apsb.2020.02.008

Xia, S., Liu, Q., Wang, Q., Sun, Z., Su, S., Du, L., Ying, T., Lu, L., & Jiang, S. (2014). Middle East respiratory syndrome coronavirus (MERS-CoV) entry inhibitors targeting spike protein. *Virus Research*, *194*, 200–210. https://doi.org/10.1016/j.virusres.2014.10.007

Yang, H., Xie, W., Xue, X., Yang, K., Ma, J., Liang, W., Zhao, Q., Zhou, Z., Pei, D., Ziebuhr, J., Hilgenfeld, R., Yuen, K. Y., Wong, L., Gao, G., Chen, S., Chen, Z., Ma, D., Bartlam, M., & Rao, Z. (2005). Design of wide-spectrum inhibitors targeting coronavirus main proteases. *PLoS Biology*, *3*(10), e324. https://doi.org/10.1371/journal.pbio.0030324

Yang, H., Yang, M., Ding, Y., Liu, Y., Lou, Z., Zhou, Z., Sun, L., Mo, L., Ye, S., Pang, H., Gao, G. F., Anand, K., Bartlam, M., Hilgenfeld, R., & Rao, Z. (2003). The crystal structures of severe acute respiratory syndrome virus main protease and its complex with an inhibitor. *Proceedings of the National Academy of Sciences of the United States of America*, *100*(23), 13190–13195. https://doi.org/10.1073/pnas.1835675100

Zaki, A. M., Van Boheemen, S., Bestebroer, T. M., Osterhaus, A. D., & Fouchier, R. A. (2012). Isolation of a novel coronavirus from a man with pneumonia in Saudi Arabia. *The* New *England* Journal of Medicine, *367*(19), 1814–1820. https://doi.org/10.1056/NEJMoa1211721

Zhong, N., Zhang, S., Zou, P., Chen, J., Kang, X., Li, Z., Liang, C., Jin, C., & Xia, B. (2008). Without its N-finger, the main protease of severe acute respiratory syndrome coronavirus can form a novel dimer through its C-terminal domain. *Journal of Virology*, *82*(9), 4227–4234. https://doi.org/10.1128/JVI.02612-07

Zhu, N., Zhang, D., Wang, W., Li, X., Yang, B., Song, J., Zhao, X., Huang, B., Shi, W., Lu, R., Niu, P., Zhan, F., Ma, X., Wang, D., Xu, W., Wu, G., Gao, G. F., & Tan, W. (2020). A novel coronavirus from patients with pneumonia in China, 2019. *The* New *England* Journal of Medicine, *382*(8), 727–733. https://doi.org/10.1056/NEJMoa2001017

Zumla, A., Chan, J. F., Azhar, E. I., Hui, D. S., & Yuen, K.-Y. (2016). Coronaviruses - drug discovery and therapeutic options. *Nature Reviews. Drug Discovery*, *15*(5), 327–347. https://doi.org/10.1038/nrd.2015.37